Ocean Dynamics (2016) 66:1379–1413
DOI 10.1007/s10236-016-0988-1

Meteorology and oceanography of the Atlantic sector of the Southern Ocean—a review of German achievements from the last decade

Hartmut H. Hellmer[1] · Monika Rhein[2] · Günther Heinemann[3] · Janna Abalichin[4] · Wafa Abouchami[5] · Oliver Baars[6] · Ulrich Cubasch[4] · Klaus Dethloff[7] · Lars Ebner[3] · Eberhard Fahrbach[1] · Martin Frank[8] · Gereon Gollan[8] · Richard J. Greatbatch[8] · Jens Grieger[4] · Vladimir M. Gryanik[1,9] · Micha Gryschka[10] · Judith Hauck[1] · Mario Hoppema[1] · Oliver Huhn[2] · Torsten Kanzow[1] · Boris P. Koch[1] · Gert König-Langlo[1] · Ulrike Langematz[4] · Gregor C. Leckebusch[11] · Christof Lüpkes[1] · Stephan Paul[3] · Annette Rinke[7] · Bjoern Rost[1] · Michiel Rutgers van der Loeff[1] · Michael Schröder[1] · Gunther Seckmeyer[10] · Torben Stichel[12] · Volker Strass[1] · Ralph Timmermann[1] · Scarlett Trimborn[1] · Uwe Ulbrich[4] · Celia Venchiarutti[13] · Ulrike Wacker[1] · Sascha Willmes[3] · Dieter Wolf-Gladrow[1]

Received: 18 March 2016 / Accepted: 29 August 2016 / Published online: 16 September 2016

Abstract In the early 1980s, Germany started a new era of modern Antarctic research. The Alfred Wegener Institute Helmholtz Centre for Polar and Marine Research (AWI) was founded and important research platforms such as the German permanent station in Antarctica, today called Neumayer III, and the research icebreaker *Polarstern* were installed. The research primarily focused on the Atlantic sector of the Southern Ocean. In parallel, the German Research Foundation (Deutsche Forschungsgemeinschaft, DFG) started a priority program 'Antarctic Research' (since 2003 called SPP-1158) to foster and intensify the cooperation between scientists from different German universities and the AWI as well as other institutes involved in polar research. Here, we review the main findings in meteorology and oceanography of the last decade, funded by the priority program. The paper presents field observations and modelling efforts, extending from the stratosphere to the deep ocean. The research spans a large range of temporal and spatial scales, including the interaction of both climate components. In particular, radiative processes, the interaction of the changing ozone layer with large-scale atmospheric circulations, and changes in the sea ice cover are discussed. Climate and weather forecast models provide an insight into the water cycle and the

Responsible Editor: Jörg-Olaf Wolff

✉ Hartmut H. Hellmer
Hartmut.Hellmer@awi.de

[1] Alfred-Wegener-Institut Helmholtz-Zentrum für Polar- und Meeresforschung, Bremerhaven, Germany

[2] Institut für Umweltphysik IUP - Zentrum für Marine Umweltwissenschaften MARUM, Universität Bremen, Bremen, Germany

[3] Environmental Meteorology, Universität Trier, Trier, Germany

[4] Institut für Meteorologie, Freie Universität Berlin, Berlin, Germany

[5] Max Planck Institut für Chemie, Mainz, Germany

[6] Department of Geosciences, Guyot Hall, Princeton, NJ 08544, USA

[7] Alfred-Wegener-Institut Helmholtz-Zentrum für Polar- und Meeresforschung, Potsdam, Germany

[8] GEOMAR Helmholtz-Zentrum für Ozeanforschung Kiel, Kiel, Germany

[9] A.M. Obukhov Institute of Atmospheric Physics, Russian Academy of Sciences, Moscow, Russia

[10] Institut für Meteorologie und Klimatologie, Leibniz Universität Hannover, Hannover, Germany

[11] School of Geography, Earth and Environmental Sciences, University of Birmingham, Birmingham, UK

[12] Ocean and Earth Science, National Oceanographic Centre Southampton, University of Southampton, Southampton, UK

[13] Joint Research Centre (JRC) - European Commission's Science Service, Brussels, Belgium

climate change signals associated with synoptic cyclones. Investigations of the atmospheric boundary layer focus on the interaction between atmosphere, sea ice and ocean in the vicinity of polynyas and leads. The chapters dedicated to polar oceanography review the interaction between the ocean and ice shelves with regard to the freshwater input and discuss the changes in water mass characteristics, ventilation and formation rates, crucial for the deepest limb of the global, climate-relevant meridional overturning circulation. They also highlight the associated storage of anthropogenic carbon as well as the cycling of carbon, nutrients and trace metals in the ocean with special emphasis on the Weddell Sea.

Keywords Polar meteorology · Polar oceanography · Antarctica · Southern Ocean · Weddell Sea

Abbreviations

AABW	Antarctic Bottom Water
AAIW	Antarctic Intermediate Water
AAO	Antarctic Oscillation
ABS	Amundsen-Bellingshausen Sea
ACC	Antarctic Circumpolar Current
AMPS	Antarctic mesoscale prediction system
AOGCM	Atmosphere-ocean general circulation model
AWI	Alfred Wegener Institute Helmholtz Centre for Polar and Marine Research
CAO	Cold air outbreak
CBL	Convective boundary layer
CDW	Circumpolar Deep Water
CFC	Chlorofluorocarbon
COSMO	Consortium of small-scale modelling
CTD	Conductivity-temperature-depth
DFG	Deutsche Forschungsgemeinschaft (German Research Foundation)
DOC	Dissolved organic carbon
DOM	Dissolved organic matter
DWD	German Meteorological Service
ECHAM	General circulation model of the Max Planck Institute for Meteorology (Hamburg)
EMAC	ECHAM/MESSy Atmospheric Chemistry
ERA	ECMWF reanalysis
ETC	Extra-tropical cyclone
FESOM	Finite Element Sea ice Ocean Model
FRIS	Filchner-Ronne Ice Shelf
GHG	Greenhouse gas
HIRHAM	Regional climate model combining HIRLAM and ECHAM
HIRLAM	High-resolution limited area model
HSSW	High-Salinity Shelf Water
LES	Large Eddy Simulation
LIS	Larsen Ice Shelf
MODIS	Moderate-Resolution Imaging Spectroradiometer
NAM	Northern Annular Mode
NCEP	National Centres for Environmental Prediction
NH	Northern hemisphere
OA	Ocean acidification
P-E	Precipitation minus evaporation
PACC	Potential anthropogenic climate changes
SAM	Southern Annular Mode
SAMW	Subantarctic Mode Water
SH	Southern hemisphere
SIC	Sea ice concentration
SIE	Sea ice extent
SPP	Schwerpunktprogramm (DFG Priority Program)
SZA	Solar zenith angle
UV	Ultraviolet
WDW	Warm Deep Water
WMO	World Meteorological Organization
WSBW	Weddell Sea Bottom Water
WSDW	Weddell Sea Deep Water

1 Introduction

Two hundred years ago, the Southern Ocean was viewed as an inaccessible, stormy and icy sea, challenging dauntless explorers, hunters and whalers. Today, the Southern Ocean is considered to be an important tessera of the climate puzzle hosting numerous processes of global importance. It connects the three major oceans through the most vigorous ocean current on Earth, the Antarctic Circumpolar Current, ventilates most of the world ocean abyss, participates in the global carbon cycle and affects the rate of global sea level rise due to the interaction with the Antarctic Ice Sheet. However, the Southern Ocean not only acts but also reacts to sea floor topography and the polar atmosphere. The former guides currents around the continent, warm waters of open ocean origin into ice shelf cavities, dense shelf waters down the continental slope and determines the kind of water able to escape the basins of the marginal seas. The latter provides energy for driving the ocean currents, controls the surface fluxes of heat and moisture, regulates the exchange of natural and anthropogenic gases and determines sea ice properties and coverage with consequences for primary production, ocean-air fluxes and water mass characteristics. The atmosphere links air-ice-ocean interaction with the stratosphere, e.g. changes in stratospheric circulation, due to ozone loss, to tropospheric circulations and sea ice coverage. Furthermore, the atmosphere is the fastest connection between Antarctica and the mid-latitudes, and the tropics.

It is the interplay between both components of the climate system, which restricts scientific surveys in the Southern Ocean mainly to the austral summer season, and even then, the access to the continental shelves of the marginal seas is limited. The combination of results from the few expeditions

to the Antarctic coast, the increasing capability of satellite sensors, and the progress achieved in terms of numerical model development revealed that the continental shelves are the prime locations for sea ice formation due to intense ocean heat loss to the cold atmosphere. Concentrated in coastal polynyas, the resulting brine rejection causes a densification of the continental shelf water. This water mass either contributes to the formation of deep and bottom water or participates in the sub-ice shelf circulation providing the heat for basal melting. The meltwater input influences the stability of the shelf water column with consequences for sea ice cover, for air-sea fluxes and for the characteristics of the deep and bottom waters. The main source region for both water masses is the southern extreme of the Atlantic Ocean, the Weddell Sea (Fig. 1). Due to the ocean ridges fringing the Weddell Basin, only Weddell Sea Deep Water escapes via several deep passages and feeds the Antarctic Bottom Water, historically assumed to be the source for most of the abyssal waters.

Due to the potential of the Weddell Sea region for innovative discoveries and the relative vicinity to home ports, past (W. Filchner, *Deutschland* Expedition, 1911–1913) and recent German investigations focussed on the Weddell Sea and the fringing continent including ice shelves and the hinterland. Since 1981, continental research in the Weddell Sea area is based on the *Ekstrømisen* at the German permanent station, today called 'Neumayer III', and the summer Kohnen Station on Drauning Maud Land (Fig. 1). Since 1982, expeditions to the Weddell Sea (and beyond) are supported immensely by the icebreaker *Polarstern*, which provides the platform for multidisciplinary polar research even during the austral winter months. Two research aircraft are available for scientific campaigns during the summer season. These research platforms (stations, icebreaker, aircraft) are run by the Alfred Wegener Institute Helmholtz Centre for Polar and Marine Research (AWI) and allow the operation of modern devices ranging from ROVs to recently used unmanned air vehicles (UAV, Jonassen et al. 2015) for atmospheric boundary layer research.

Here, we review the achievements of recent investigations of the polar atmosphere and ocean with the focus on the Weddell Sea, primarily funded by the Priority Program (Schwerpunktprogramm, SPP-1158) 'Antarctic Research' of the German National Science Foundation (Deutsche Forschungsgemeinschaft, DFG). The main aim of the SPP is to give scientists from universities access to Antarctic stations and research platforms, thereby fostering and intensifying the cooperation between scientists from different German universities and the AWI as well as other institutes worldwide involved in polar research. This paper summarizes the main findings of the last decade.

2 Climate relevant processes in the Antarctic atmosphere

The atmosphere is a key component of the Antarctic climate system. Atmospheric processes ranging from micrometres to thousands of kilometres are responsible for the interaction and transports of momentum, energy and matter at the interface of ocean and ice surfaces, exchange between tropics, mid-latitudes and the Antarctic and the exchange between stratosphere and

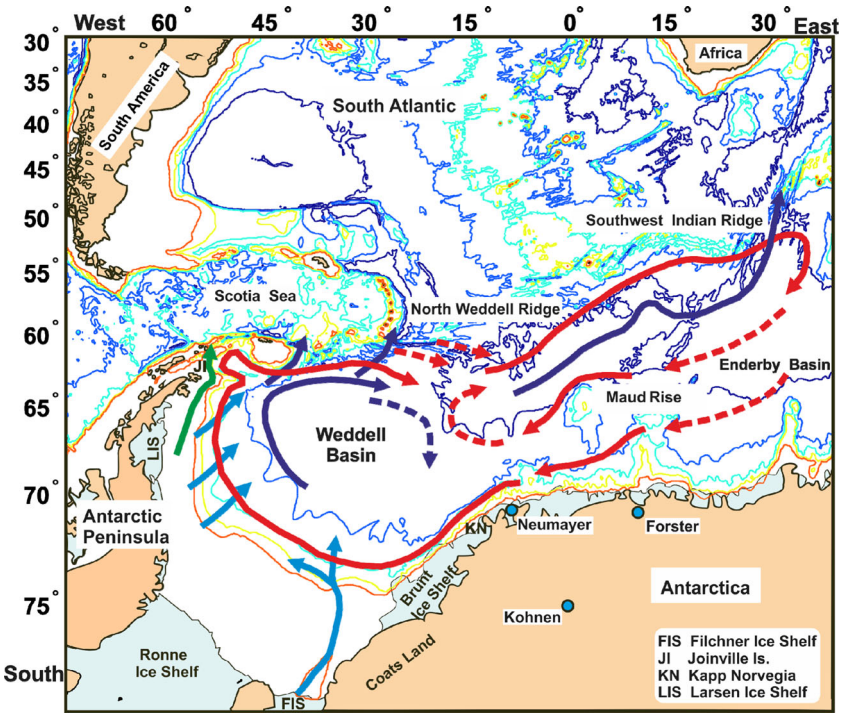

Fig. 1 Map of the Atlantic Sector of the Southern showing bottom topography, trajectories of warm deep water (WDW, *red*), Weddell sea deep water (WSDW, *dark blue*), Ice shelf water (ISW, *light blue*), and low-salinity shelf water (LSSW, *green*). Locations of one historic (Forster) and the two recent German stations on the continent as *blue dots.* Abbreviations used are listed in the *insert*

troposphere. Research in the realm of the Antarctic atmosphere contributed to the understanding of the interaction of the changing ozone layer with large-scale atmospheric circulations and changes in the sea ice cover (Section 2.1). The complex interaction between the radiation field as a function of wavelength, snow reflection and clouds was investigated (Section 2.2). Studies using climate and weather forecast models improved knowledge of the climate change signals associated with synoptic cyclones (Section 2.3) and the water cycle (Section 2.4). Investigations of the atmospheric boundary layer focused on the interaction between atmosphere, sea ice and ocean particularly for leads and polynyas (Section 2.5).

2.1 Ozone-related changes in atmospheric circulation and sea ice extent

The stratospheric ozone depletion is most evident in the ozone hole that appears each austral spring over Antarctica. The ozone depletion led to a 6 °C cooling of the lower stratosphere over the South Pole and an associated intensification of the stratospheric vortex in spring. The interaction of these stratospheric changes with the troposphere and particularly with the sea ice extent in the Antarctic was a focus of international research during the last decade. Since 1992, weekly ozone soundings have been performed at the German Antarctic research station Neumayer (König-Langlo and Loose, 2007). These measurements continue the time series that started already in 1985 at the neighbouring German research base Georg-Forster-Station (König-Langlo and Gernandt, 2009). Ozone sensors (ECC 5A/6A) mounted on RS80/RS90/RS92 radiosondes (Vaisala) have been used. High ozone partial pressures are measured at altitudes around 20 km—called 'ozone layer'—from December/January to the end of August. During Antarctic spring (September to November), the ozone layer vanishes more or less completely.

This Antarctic springtime ozone depletion shows remarkable interannual variations (Fig. 2). From 1985 to about 2006, an overall reduction of the ozone partial pressure in the ozone layer is obvious. The ozone reduction is strongly correlated with a cooling of the stratosphere. Corresponding variations or a significant trend during other seasons could not be ascertained. A biennial oscillation of the springtime ozone concentrations is evident from 1985 until 1989. Labitzke and Van Loon (1992) explained this behaviour as dynamically induced from the quasi-biennial oscillation of stratospheric wind above the equator. In the 1990s, the biennial oscillation of the spring ozone concentration was not measured any longer. The data showed a more or less continuous reduction of the ozone concentration and a cooling of the air around 70 hPa. Crutzen and Arnold (1986) explained this behaviour as a chemical effect caused by the worldwide rising anthropogenic chlorofluorocarbon (CFC) concentrations.

Between 2001 and 2004, the overall springtime ozone concentrations measured above an altitude of 20 km were rising again. This effect was interpreted as the beginning of the recovery of the 'ozone hole' as a response to the worldwide ban of nearly any CFC product in the Montreal Protocol in 1987. However, the measurements in the following years from Neumayer II (Hoppel et al. 2005) showed that the recovery of the ozone hole did not start at that time. Especially the very high temperatures and ozone concentrations during Spring 2002 (Fig. 2) could be explained as a consequence of a dynamic breakdown of the Antarctic stratospheric vortex during winter. It took a whole decade until the measurements from Neumayer and other Antarctic stations indicated an ongoing recovery of the ozone layer. In September 2014, the World Meteorological Organization (WMO) officially posted the success of the Montreal Protocol from 1987 (WMO 2014). However, the observed increase of global annual mean total ozone of 1 % between 2000 and 2013 compared to the large

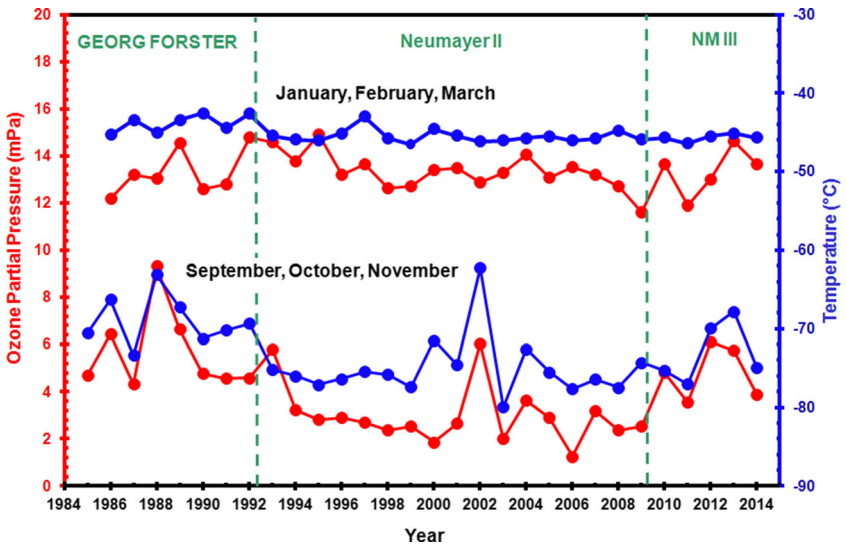

Fig. 2 Time series of the average ozone partial pressure (*red*) and temperature (*blue*) at 70 hPa at the stations Georg-Forster and Neumayer covering the period 1985 to 2014

interannual variability found in that time period did not allow to conclude a recovery of the Antarctic ozone.

The trends of sea ice extent (SIE) during the last decades are different for both hemispheres. Arctic sea ice has dramatically decreased in the recent past. Estimates from satellite measurements find a negative trend of about 10 % per decade since 1979 (Comiso et al. 2008). In contrast, annual mean Antarctic sea ice increased by about 1 % per decade for the years 1978–2006 (Turner et al. 2009). While the Arctic sea-ice retreat has been associated with the warming of the troposphere caused by increasing greenhouse gas (GHG) concentrations (IPCC 2013), the ozone depletion by man-made halogens in the polar stratosphere and its impact on tropospheric circulation have been suggested as the driving mechanism to explain the observed Antarctic changes (e.g. Thompson and Solomon 2002). However, there is still low confidence in the scientific understanding of the observed increase in Antarctic SIE since 1979, due to missing knowledge of internal variability and competing explanations for the causes of change (IPCC 2013). With further increasing GHGs and an expected recovery of polar ozone at the end of the twenty-first century, projections of future polar climate and its hemispheric differences are highly uncertain. To understand and project the interactions between the atmosphere, oceans and the cryosphere as well as the chemical and radiative effects of natural and anthropogenic climate gases throughout the troposphere and stratosphere, complex numerical models need to be applied. A new atmosphere-ocean version of the ECHAM/MESSy Atmospheric Chemistry (EMAC) chemistry-climate model was used in a study, which combines the EMAC model (Jöckel et al. 2006) with the Max Planck Institute-Ocean Model (MPI-OM, Jungclaus et al. 2006).

The coupled atmosphere-ocean system is characterized by unforced internal variability on different time scales, as is evident in a 110-year EMAC simulation that was integrated under fixed boundary conditions for the year 1960. The analysis begins for austral winter (June/July/August, JJA), using the Southern Annular Mode (SAM) index at 850 hPa and JJA mean SIE around Antarctica. The SAM is the dominant mode of low frequency variability in the southern hemisphere atmosphere, a positive/negative SAM being associated with stronger/weaker westerly winds (Thompson and Wallace 2000). The analysis reveals a positive correlation between the SAM index and SIE on interannual time scales, while a significant correlation at low frequencies was not found (Fig. 3). The positive correlation between the SAM and SIE at interannual time scales is consistent with observations. It has been suggested to result from stronger westerlies during positive SAM that insulate the high latitudes from exchange with the lower latitudes and lead to an overall cooling of the Antarctic region, even though some areas may also experience higher temperatures and less sea ice during a positive SAM like the Antarctic Peninsula (e.g. Thompson and Solomon 2002). However, the lack of correlation between the SAM and SIE at low frequencies in the model does not support the hypothesis that the observed trend towards the positive polarity of the SAM can explain the observed increase in sea ice.

A comparative analysis of the Arctic region reveals a similar behaviour on interannual time scales (not shown) in which the SIE is positively correlated with the Northern Annular Mode (NAM)—the northern hemisphere equivalent of the SAM—consistent with previous studies (e.g. Rigor et al. 2002). However, on time scales longer than 11 years a much more coherent pattern of behaviour emerges in which periods of a positive polarity of the NAM are associated with reduced SIE and vice versa (not shown). This happens because the NAM is an important driver for the Atlantic meridional overturning circulation (Eden and Jung 2001); and on time scales longer than 11 years, an enhanced overturning warms the high northern latitudes leading to reduced SIE.

Figure 4a shows the evolution of Antarctic SIE between 1960 and 2100, as simulated with the EMAC model assuming a continuing future increase of GHG concentrations according to the RCP6.0 scenario (IPCC 2013) and projected emissions of ozone depleting substances following the WMO A-1 scenario. During the period of strongest Antarctic ozone depletion (about 1980–2007), the SIE shows considerable interannual variability but no indication of a retreat comparable to the Arctic. The local changes in sea ice concentration (SIC) around Antarctica in this period agree with observations (e.g. Turner et al. 2009): Consistent with an intensification of the Amundsen-Bellingshausen Sea (ABS) low, enhanced northerly winds induce a reduction of SIC in the ABS, while stronger southerlies lead to a larger SIC in the Ross Sea. An even stronger SIC enhancement was found in the Weddell Sea (left panel in Fig. 4b). These changes arise from two contributions: (a) an increase of the SAM associated with the intensification of the stratospheric polar vortex during Antarctic ozone depletion and a concurrent reduction in planetary wave activity and (b) enhanced synoptic activity due to climate change. In the upcoming decades (2008–2054, middle panel in Fig. 4b), i.e. a period with increasing climate change and declining yet still relevant ozone depletion, the SIC increases over the Ross and Weddell Seas are weaker. However, in the second half of the twenty-first century (2055–2096, right panel in Fig. 4b), when total column ozone is projected to recover, the GHG induced climate change will dominate and Antarctic SIC is projected to reduce, similar to the Arctic. While the spatial signatures of past SIE changes in EMAC are consistent with observations, the largest modelled changes occur in austral winter and spring, in contrast to autumn in the measurements. More analysis is also required to separate and quantify the relative impacts of ozone and GHG changes on Antarctic sea ice and, in general, polar climate.

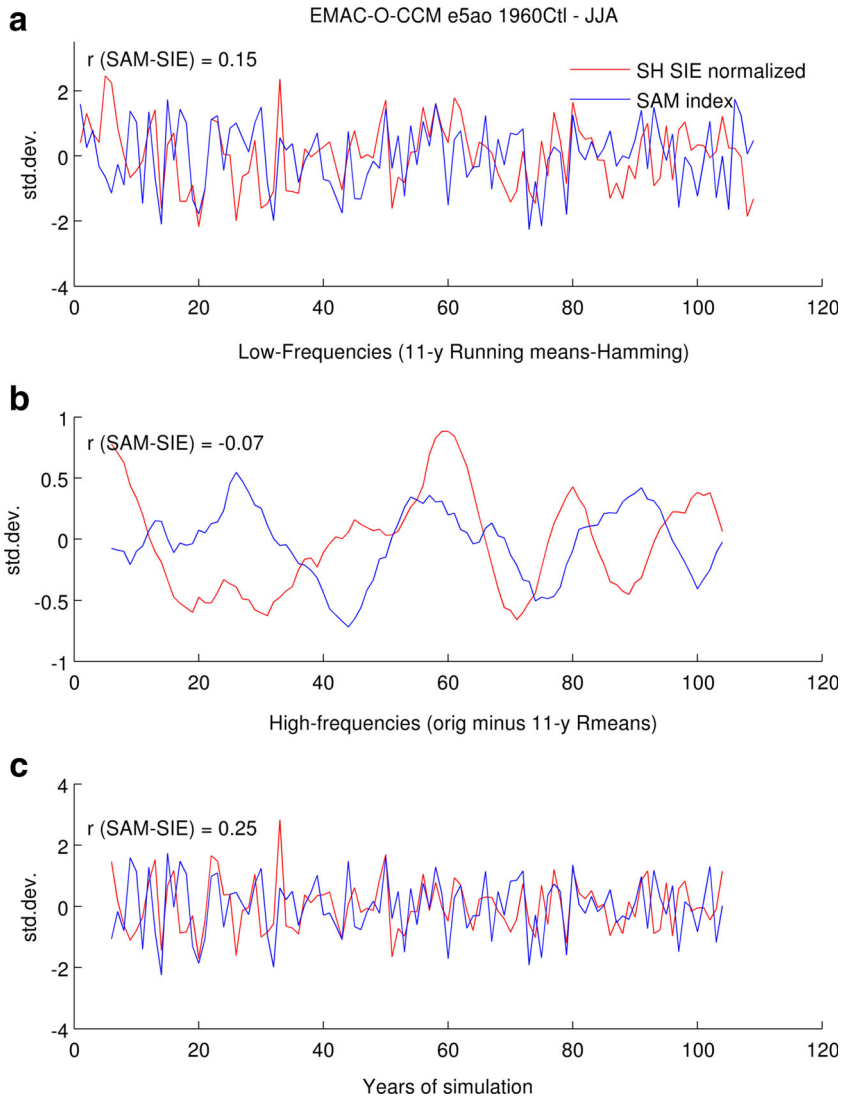

Fig. 3 **a** Normalized JJA mean time series of the southern hemisphere sea ice extent SIE (i.e. SIE is divided by its interannual standard deviation, about 0.9×10^6 km^2) and the SAM (defined as in Thompson and Wallace 2000) in the control run of EMAC-O-CCM. **b** 11-y running means using Hamming window. **c** Shows (**a**) minus (**b**). Correlation values between the time series are indicated in the *upper left* of each panel

2.2 Progress in the measurements of sky luminance and sky radiance

Variations in the ozone concentrations have a strong impact on the incoming radiation on the earth surface. It is well known that the direct impact is strongly wavelength-dependent. While the influence of ozone concentrations on the radiation is weak in the visible part of the spectrum, it can be dominant in parts of the infrared and in the shortwave ultraviolet (UV) spectrum. An improved understanding of the radiation is therefore helpful to determine the impact of current and future changes on the climate in Antarctica. Angular distribution of solar radiance and its spectral characteristics are key radiative quantities to study the impact of climate changes in Antarctica (Cordero et al. 2013, 2014). These quantities and the absorption characteristics of snow determine how much radiation is reflected back to space and how much snow melts should temperatures rise.

In the last decade, the observational capabilities for measuring radiance and luminance were significantly improved. In contrast to the 'old' scanning instruments that needed one day to measure the spectral radiance field, the newly developed instruments are now capable to measure sky radiance in dependence of zenith and azimuth angle in more than 100 directions simultaneously within a second (Riechelmann et al. 2013; Tohsing et al. 2013; Seckmeyer et al. 2010). These instruments have already improved our understanding of climate change in both the Arctic and Antarctic, and we expect that also for the future.

Sky luminance and spectral radiance have been characterized at the Neumayer Station during the austral summer 2003/2004 (Wuttke and Seckmeyer 2006). The high reflectivity of the surface (albedo) in Antarctica, reaching values up to 100 % in the UV and visible part of the solar spectrum due to snow cover (Wuttke et al. 2006) modifies the radiation field considerably when compared to mid-latitudes. A dependence

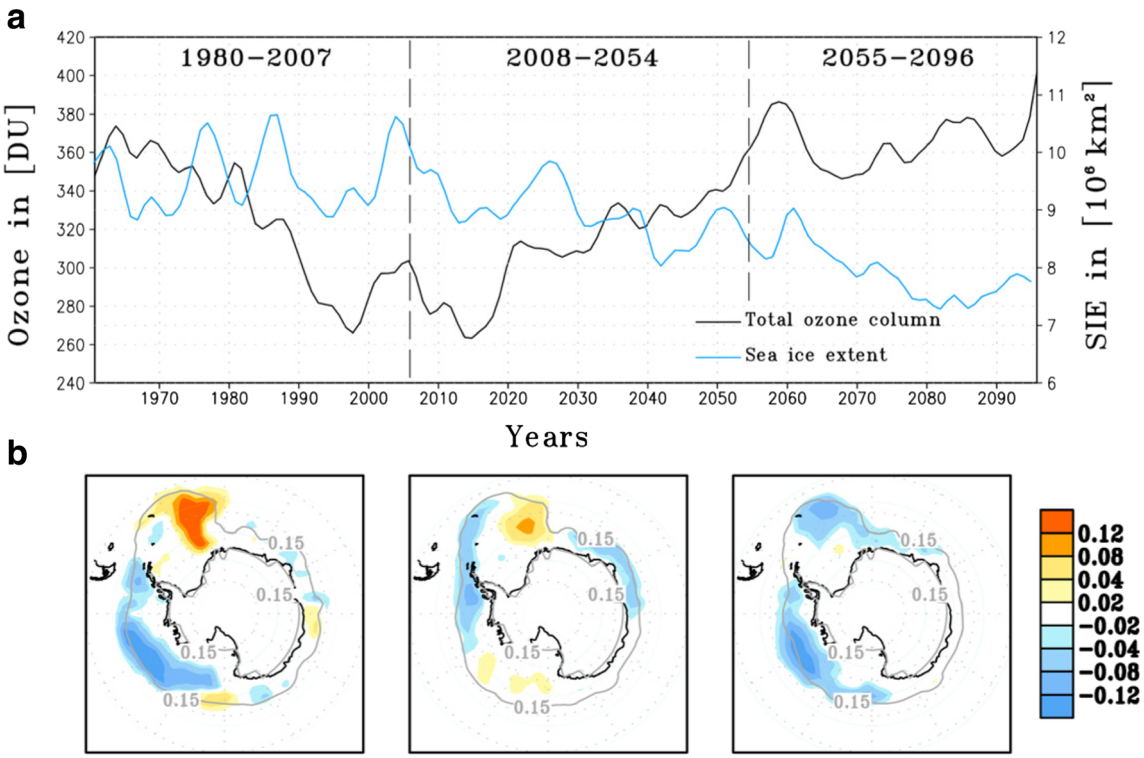

Fig. 4 **a** Evolution of the Antarctic total ozone column (in Dobson Unit, DU, 60° S–90° S mean, *black*) in October and Antarctic sea ice extent (SIE, in km^2, *blue*) in December between 1960 and 2100, simulated with the EMAC chemistry-climate model, assuming the RCP6.0 greenhouse gas scenario and the WMO-A1 scenario for ozone depleting substances. The time series have been smoothed by applying three times a 1-2-1 filter. **b** Decadal trends in sea ice concentration (SIC) in October for the periods 1980–2007 (*left*), 2008–2054 (*middle*), and 2055–2096 (*right*). Grid boxes with SIC >0.15 are considered as covered with sea ice

of luminance and spectral radiance on solar zenith angle (SZA) and surface albedo was identified. For snow and cloudless sky, the horizon luminance exceeds the zenith luminance by as much as a factor of 8.2 and 7.6 for a SZA of 86° and 48°, respectively. Thus, a snow surface with high albedo can enhance horizon brightening compared to grass by a factor of 1.7 for low sun at a SZA of 86° and by a factor of 5 for high sun at a SZA of 48°. Measurements of spectral radiance show increased horizon brightening for increasing wavelengths and, in general, a good agreement with model results. However, large deviations are found between measured and modelled values especially in the infrared range that are only partly explained by measurement uncertainties. Progress is expected by future studies with the faster instruments available now.

2.3 Extra-tropical cyclones and storms and their impact on the southern polar hemisphere

Extra-tropical cyclones (ETCs) in the mid to high latitudes of the southern hemisphere (SH) are a fundamental part of the atmospheric energy and momentum transport. ETCs are essential for the meridional exchange processes, which are necessary to maintain the hemispheric and, thus, global energy balance of the Earth's climate system. In contrast to the northern hemisphere, where stationary waves in the mid-troposphere are important for the poleward energy transport, the atmospheric energy transport in the SH is mainly accomplished by transient and shorter baroclinic waves, evident as travelling ETCs at the surface. In the absence of orographic influences, which lead to distinct areas of baroclinic cyclogenesis in the northern Atlantic and Pacific, the SH transient waves have a more circumpolar distribution. At present, potential anthropogenic climate changes (PACC) are investigated by means of a multi-model ensemble of state-of-the-art coupled atmosphere-ocean general circulation model (AOGCM) simulations, especially to understand the nature and causes of potential changes in future ETCs and their impact on Antarctica.

Most individual models as well as the ensemble mean are able to reproduce the general ETC characteristics of the SH. Nevertheless, a large model-to-model variability is revealed with respect to the quantity of simulated ETCs. Grieger et al. (2014) used a new scaling approach to account for these systematic biases. Applying the SRES A1B scenario (e.g. Nakicenovi et al. 2000) the total number of cyclones decreases at the end of the twenty-first century (due to stronger warming of the lower troposphere in polar regions one would expect less net energy transport). However, the majority of analysed AOGCMs (Fig. 5) diagnose an increased number of extremely strong ETCs. This general change is associated with a

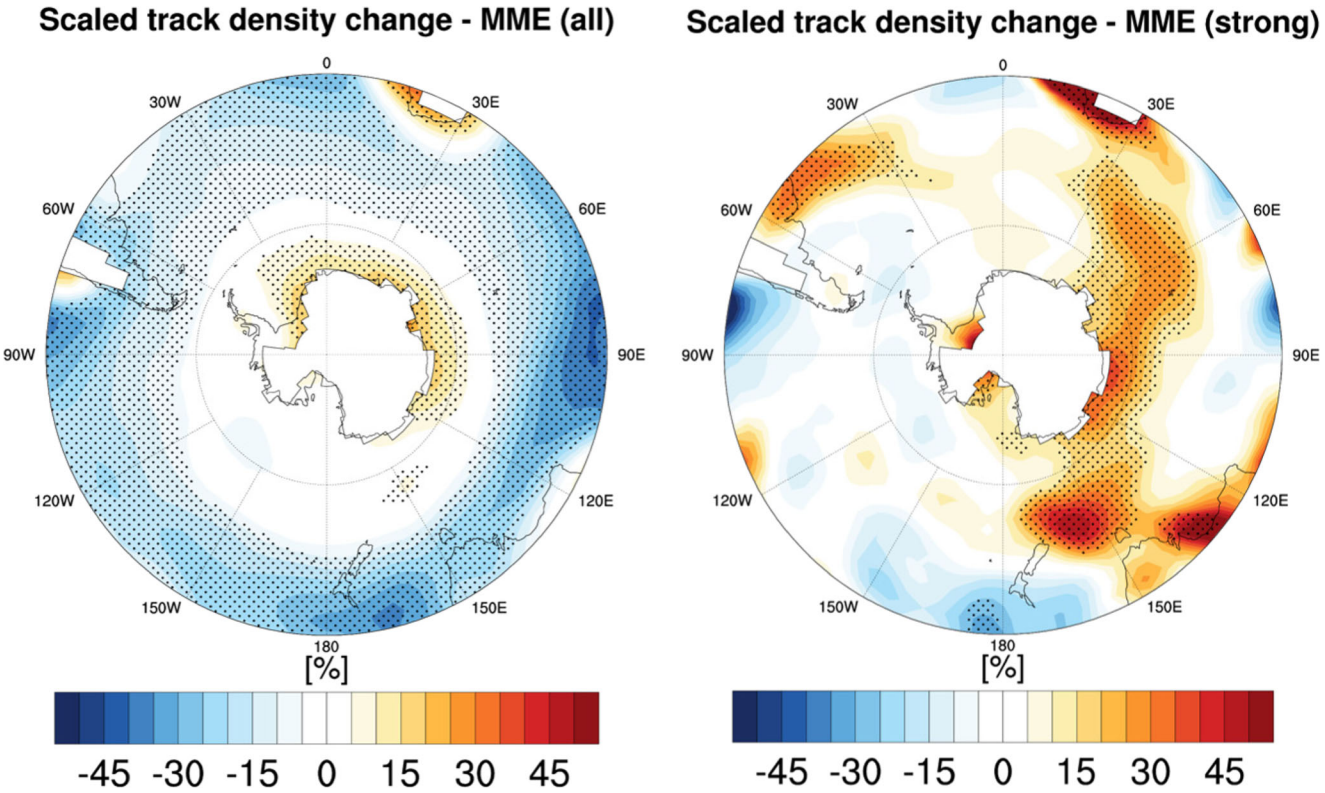

Fig. 5 Relative climate change signal [%] of the multi-model ensemble cyclone track density (April–September) for all (*left*) and strong (*right*) cyclones. Stippled areas indicate significant changes ($p < 0.05$) with respect to a Student's *t* test (Figure adopted from Grieger et al. 2014)

poleward shift related to upper tropospheric tropical warming and shifting meridional sea surface temperature gradients in the Southern Ocean (Grieger et al. 2014). The largest increase of strong cyclone activity was found in the eastern hemisphere.

The potential anthropogenic climate change also impacts poleward moisture fluxes in the SH. Distinguishing between thermodynamic and dynamic influences of PACC on moisture fluxes, PACC signals of the responsible waves in the synoptic scale show a poleward shift related to the poleward shift of ETCs (Grieger et al. 2015). Antarctic net precipitation was calculated by means of the vertically integrated moisture flux. Grieger et al. (2015) found signals of increasing net precipitation whereas the dynamical part of net precipitation decreased. They explained these findings with the low variability of synoptic-scale waves, which generally decreased, especially off the coast of West Antarctica, and suggested that this is related to a changing variability of the ABS low.

Another factor potentially changing Antarctic surface climate, is the SH springtime ozone depletion since the mid-1980s. It has its strongest impact during the austral summer months (DJF) due to a slow downward propagation of ozone hole induced anomalies in temperature, geopotential height, and wind fields. Stronger zonal surface winds were supposed to isolate the Antarctic vicinity, inducing a cooling signal in surface temperature (Gillett and Thompson, 2003). Simulations with the ECHAM/MESSy Atmospheric Chemistry model show, however, an enhancement of Antarctic surface temperature in the recent past (1960 to 2000) (Fig. 6, top left). The warming of the Antarctic surface climate, which is in good agreement with recently published observational studies (Steig et al. 2009; Schneider et al. 2012), is due to climate change by increasing GHG concentrations. It is found to be a consequence of enhanced meridional heat transport by synoptic waves (Fig. 6, top right), associated with an increased storm track density around Antarctica (not shown). The contribution to the heat flux by planetary waves (Fig. 6, top middle), however, is strongly reduced (consistent with stronger zonal winds, Fig. 6, top left). Due to the occurrence of the ozone hole, synoptic heat fluxes near the surface are suppressed, and the decrease in the planetary heat flux throughout the troposphere predominates (Fig. 6, lower middle), leading to a subsequent cooling of the continent. These results illustrate a counteraction of different climate drivers (enhanced sea-surface temperatures due to climate change and recurring springtime ozone hole), leading to a two-way impact on the characteristics of SH extra-tropical waves with a more or less pronounced enhancement of synoptic heat transport. However, more impacts have to be taken into account to fully explain the observed recent Antarctic surface changes, such as reduced radiative input due to cloud

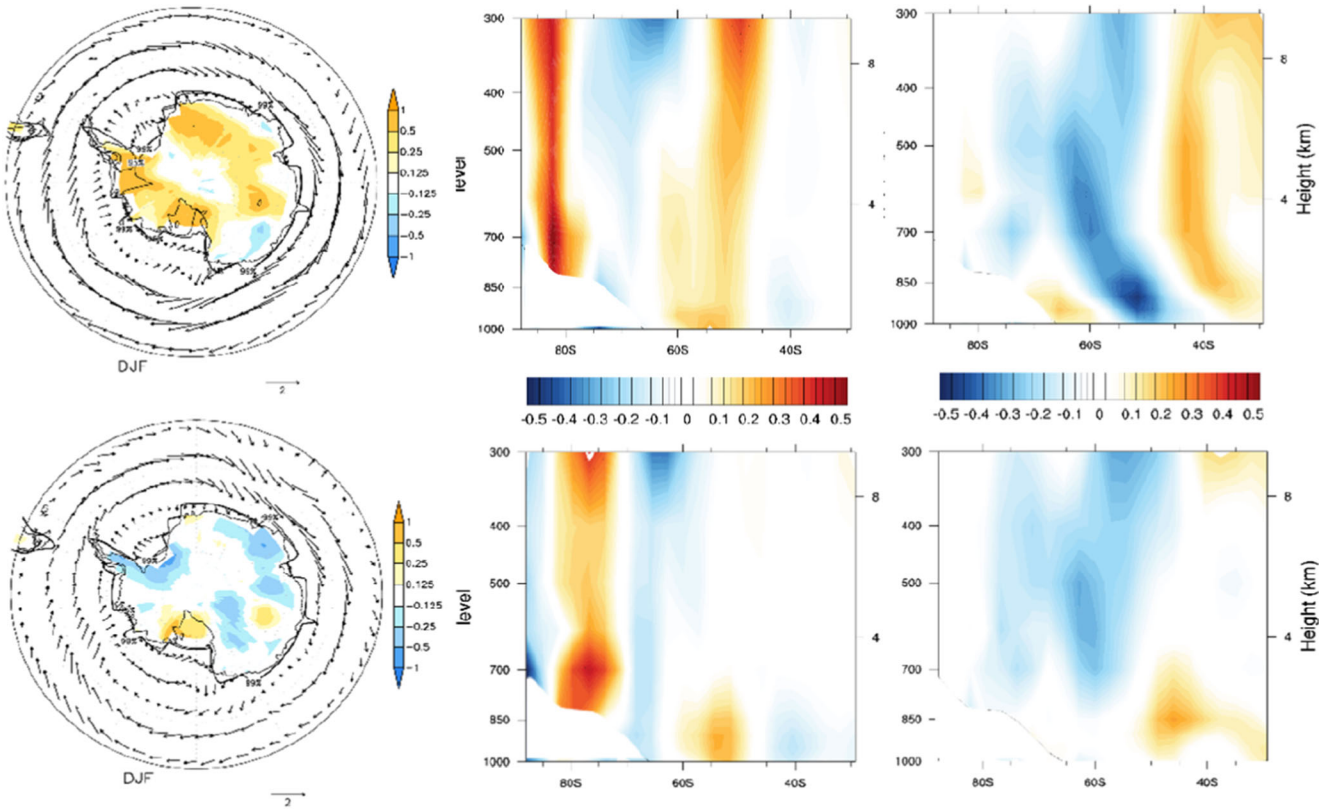

Fig. 6 Past changes (1960–2000) in surface temperature and wind [in K and m/s, *left panels*], zonal mean heat flux from planetary (*middle panels*) and synoptic (*right panels*) waves [in km/s] in DJF. *Blue shades* denote a cooling in surface temperature and an enhancement in heat fluxes. The analyses are based on 20-year time slice simulations under respective conditions. The *top row* shows the climate change signal due to rising GHGs and stratospheric ozone depletion. The *bottom row* shows the response to stratospheric ozone depletion only

cover changes with increased cyclone activity, or changes in regional wind systems, such as katabatic winds.

2.4 Components of the water cycle and their role for ice and snow accumulation

Precipitation is the dominant term among the various components of surface snow accumulation. Information from in situ observations for precipitation events are hardly available due to the difficulties in measuring precipitation under Antarctic conditions, even when using automatic weather stations (e.g. van den Broeke et al. 2004; Welker et al. 2014). Therefore, an annual snow accumulation climatology has been frequently used as an indicator for precipitation (King and Turner 1997). Later on, precipitation climatologies have been derived from model data, such as reanalysis data (Bromwich et al. 2011), mesoscale weather forecasts using the Antarctic Mesoscale Prediction System (Bromwich et al. 2005) as shown by Schlosser et al. (2008) or by regional climate models (van de Berg et al. 2006; Lenaerts et al. 2012). Recently, Palerme et al. (2014) have used satellite products from CloudSat to derive precipitation. Highest precipitation rates of more than 500 mm per year were found along the coastal escarpment; on the ice sheet plateau, the rates drop to less than 100 mm per year.

2.4.1 Precipitation processes related to synoptic disturbances

Large portions of precipitation in the coastal regions fall during episodes of passing fronts of cyclonic systems (King and Turner 1997). If precipitation, and hence the accumulation, occurs preferentially during particular months of the year, the temperature derived from ice core analysis will be biased towards the conditions prevailing during these days in the region around the drilling site. Thus, it is necessary to know the amount and timing of precipitation and to investigate precipitation events on short time scales with high spatial resolution.

A high spatial and temporal resolution is needed particularly for the simulation of high precipitation events. A selected weather situation, formation and horizontal distribution of clouds and precipitation in Queen Maud Land have been investigated by Wacker et al. (2009), using a high-resolution non-hydrostatic weather forecast model COSMO (consortium of small-scale modelling; Steppeler et al. 2003). This model was initially developed at the German Meteorological Service (DWD) and applied in that study for the first time for Antarctic

conditions. A 12-day episode from February 1999 is addressed, when low-pressure systems and related fronts travelled along the coast of Queen Maud Land. Emphasis was placed on the temporal evolution and horizontal distribution of clouds and precipitation in high spatial resolution (7-km horizontal mesh size).

The model captures the overall meteorological situation. The horizontal distribution of 12-day precipitation sums is shown in Fig. 7. The amount of modelled precipitation, in particular sums larger than 100 mm in some regions with steep topography, seems to be large when compared to the annual climatologies and to simulations with the Antarctic mesoscale prediction system (AMPS) or ECMWF reanalysis (ERA)-Interim reanalysis (Welker et al. 2014). The spatial precipitation distribution is dominated by topographic effects: Precipitation amount generally decreases towards the interior similar as seen in climatologies. In the high-resolution simulation, however, the decrease neither follows increasing distance from the coast nor the topographic contours. Instead, precipitation bands of some 100-km width appear on the plateau. The bands may be connected to the path of the frontal cloud systems, and may also be related to orographically induced gravity waves (see e.g. Zaengl 2005), which have been studied for long for Antarctica. Such mesoscale features can only be resolved by models with mesh sizes of 10 km or less (e.g. Valkonen et al. 2010).

Figure 8 shows time series of 6-h precipitation at a particular grid point close to Neumayer Station from the study of Wacker et al. (2009). The simulated timing of precipitation agrees with synoptic observations. The figure also illustrates some of the difficulties in precipitation modelling. The precipitation amount during the first 6 h of the forecast is systematically underestimated due to the spin-up effect. Even beyond the spin-up period two successive model runs clearly differ in the amount of precipitation falling in the overlapping period. Without observational data, we cannot tell which one is more reliable.

All mentioned studies on precipitation in Antarctica using mesoscale forecast models, show some success in the simulation of general spatial and temporal patterns. Nevertheless, all model precipitation data for Antarctica reveal deficiencies, such as the supposed overestimation (Fig. 8). This argues for a continuing effort in both numerical model development and precipitation observations.

2.4.2 Regional climate model simulations of the water cycle

Regional climate model (RCM) simulations based on HIRHAM4 (regional climate model combining high-resolution limited area model (HIRLAM) and ECHAM) have been carried out over Antarctica laterally driven by European Reanalysis data ERA-40 for four decades between 1958 and 1998. The model simulations with a horizontal resolution of 50 km provide a relative realistic simulation of the mean atmospheric circulation, baroclinic-scale weather systems, and the spatial distribution of precipitation minus sublimation structures (Dethloff et al. 2010). The associated atmospheric

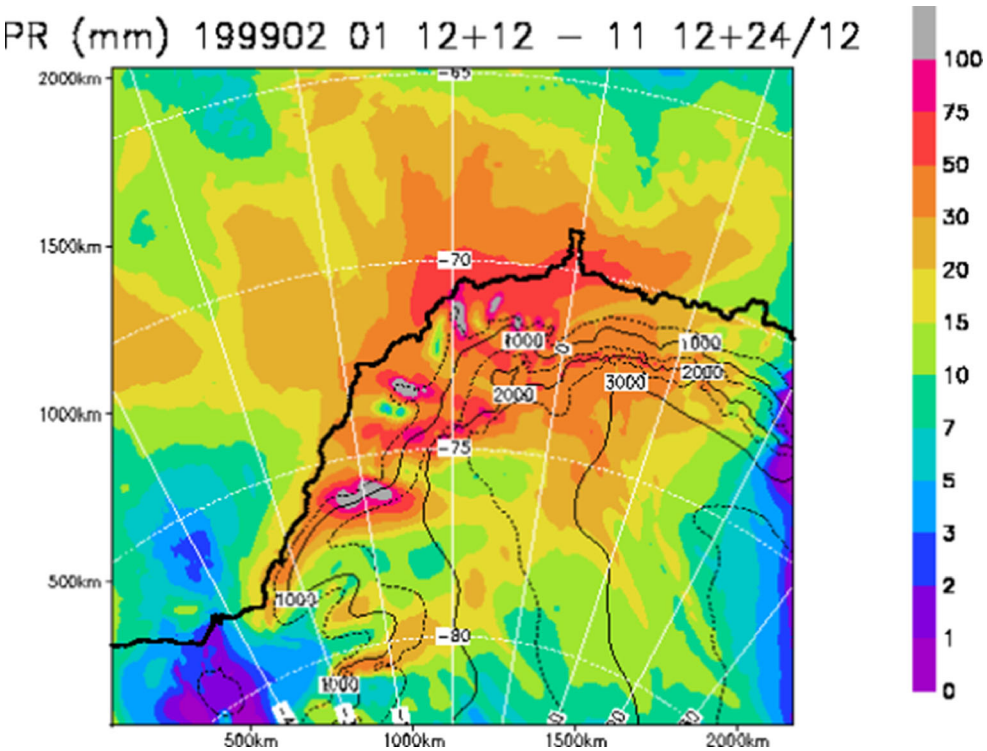

Fig. 7 Horizontal distribution of simulated precipitation sums (in mm water equivalent) for the period 2 February 12 UTC to 13 February 00 UTC, taken from successive COSMO- model runs. The runs started on 1 to 11 February 1999 each at 12 UTC. The first 12 h of each simulation are skipped as spin-up time. From Wacker et al. (2009), Figure 13b. Copyright Cambridge University Press, reprinted with permission

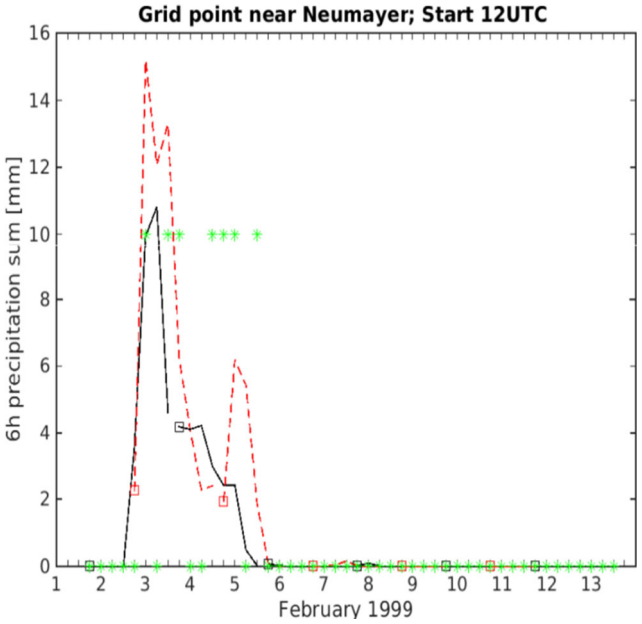

Fig. 8 Time series of simulated 6-h precipitation sums (in mm water equivalent; allocated to the final time of the period), valid at a model grid point near Neumayer Station. Results are plotted for the 48-h simulation period from COSMO model runs as used for Fig. 7. Start of a new run is marked by a *square*. Successive runs are plotted alternatively as *black solid* and *red dashed lines*. *Asterisks* mark whether the synop data report precipitation (yes >0, no =0), but they do not indicate the amount of precipitation; cases of blowing/drifting snow are excluded. Copyright Cambridge University Press, reprinted with permission

circulation and synoptic variability of the model agree with that of ERA-40, however with a pronounced internal variability (Xin et al. 2010). The computed precipitation minus evaporation (P-E) trends describe the observed surface mass accumulation increase at the West Antarctic coasts and reductions in parts of East Antarctica (Fig. 9).

The regional accumulation changes are largely driven by changes in the transient activity around the Antarctic coasts due to the varying Antarctic oscillation (AAO) phases. The monthly mean AAO index from 1958 to 1998 is based on the first principal component of the National Centres for Environmental Prediction (NCEP) 850 hPa extratropical height field (20° S–90° S) adapted from Thompson and Wallace (2000). During positive AAO, more transient pressure systems travel towards the continent; thus, West Antarctica and parts of southeastern Antarctica gain more precipitation and mass. Over central Antarctica, the prevailing anticyclone causes a strengthening of polar desertification connected with a reduced surface mass balance in the northern part of East Antarctica. The shifts in the AAO pattern is accompanied by changes in the short baroclinic waves. The associated heat and humidity fluxes (on time scales 2–6 days at 850 hPa) between positive and negative AAO periods show most pronounced shifts over the Southern Ocean. During positive AAO phases, increased heat and humidity transports, due to synoptical cyclones towards the Antarctic continent, appear over the Pacific Ocean, while over the Atlantic Ocean a reduction occurs (Dethloff et al. 2010).

2.5 The atmospheric boundary layer and interactions with sea-ice and ocean

The grid size of the newest generation of weather prediction models reaches the kilometre range and might decrease in the future to even smaller values, approaching finally the scale of

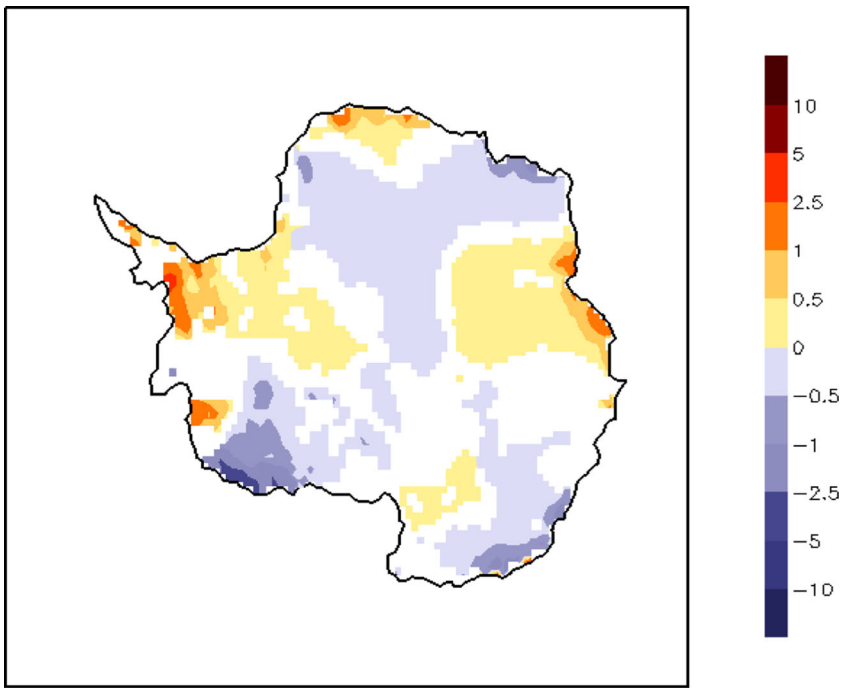

Fig. 9 Annual accumulation trends (mm/year^2) for 1992–2001 based on HIRHAM simulations. The areas of significant positive or negative changes with 95 % confidence are indicated. *White regions* describe areas below the 95 % significance level

large convective eddies in very shallow convection. The turbulent processes at grid sizes around 1 km become partly resolved and partly parameterized. When flux parameterizations in this overlapping region (often called grey zone or terra-incognita; Wyngaard (2004); Mironov (2009)) are not adjusted to the higher resolution, fluxes can be double-counted. Studies on convective mesoscale processes that occur frequently in both polar regions are presented in the following with a special focus on the difficulties related to the grey-zone problem. Due to the similar environment, process studies that have been carried out in the Arctic are very relevant for the Antarctic as well.

2.5.1 Convection over leads

The atmospheric boundary layer over closed polar sea ice is often characterized by a near-neutral or slightly stable layer of 100–300-m thickness, capped by a strong inversion. Radiative cooling or warm-air advection can even lead to surface-based inversions. However, also convective processes can occur over small cracks in sea ice, which often widen to channels or lake-like openings (leads; Fig. 10). Over leads, the large difference between air and sea surface temperature generates strong convective plumes, which interact with the stably stratified environment (see, e.g. the review paper by Vihma et al. (2014)). The strong unstable stratification over the leads with Obukhov lengths down to 0.11 m (Andreas and Cash 1999) causes heat fluxes (up to several hundred W m^{-2}). Therefore, they have to be taken into account in the calculation of the surface energy budget even when the area fraction of leads is often not greater than 1–5 %. Although the effect of single leads can be small, the integral effect of a lead ensemble in a large region can increase the near-surface temperature of a drifting air parcel by several Kelvin when the sea ice concentration changes by 1 % only (Lüpkes et al. 2008a).

Thus, it is important to account for convection over leads in climate models. The horizontal scale of leads and plumes is much below the grid size of climate models so that the fluxes over grid boxes with partial sea ice coverage usually depend linearly on the sea ice concentration. However, Andreas and Cash (1999) emphasize that fluxes per unit area are larger over small leads than over large ones, and Lüpkes and Gryanik (2015) show that the transfer of momentum and heat depends nonlinearly on sea ice concentration.

The treatment of convection over leads is not only difficult with respect to surface fluxes, the processes above the surface layer are also complex as shown by, e.g. Lüpkes et al. (2008b) and Esau (2007). One reason is the strong horizontal non-homogeneity related to the developing plume, which consists of thermals drifting with the mean wind. The inclination of this plume (Fig. 11) depends on wind and the buoyancy flux. While there are large upward heat fluxes within the plume, cooling over ice causes also a slightly stably stratified layer with small downward heat fluxes below the plume. Lüpkes et al. (2008b) used the Large Eddy Simulation (LES) model PALM with 10-m grid size for a detailed modelling of the turbulent processes over leads and compared the results with those of the mesoscale model METRAS (Schlünzen 1990). The latter was run with a grid size of 200 m, which resolves the plume but not the smaller eddies (thermals) as the LES does. A good agreement of both model results could only be obtained when METRAS was used with a new turbulence closure accounting for the effects of horizontal non-homogeneity caused by the convective plume. It combines a local closure outside the plume region with a non-local closure inside the plume. For the non-local closure, a new scaling was suggested which is based on the vertically integrated mean horizontal velocity at the lead's upstream edge, on the surface buoyancy flux over the lead, and on the internal convective boundary layer height (upper boundary of plume). In contrast, the traditional scaling assuming horizontal homogeneity did not work for this resolution.

The application of the new closure showed that regions of down-gradient transport and counter-gradient transport are well reproduced as in the corresponding LES (Fig. 11). Hence, a good agreement resulted also for the wind and temperature fields (see Lüpkes et al. 2008b), which were strongly affected by the convection over leads. These investigations

Fig. 10 Lead observed over the Barents Sea near Svalbard in April 2007 (Photo: C. Lüpkes). Its estimated width is 100 m. Due to relatively warm air temperatures around −10 °C only very little sea smoke, often indicating the convective plume, developed here

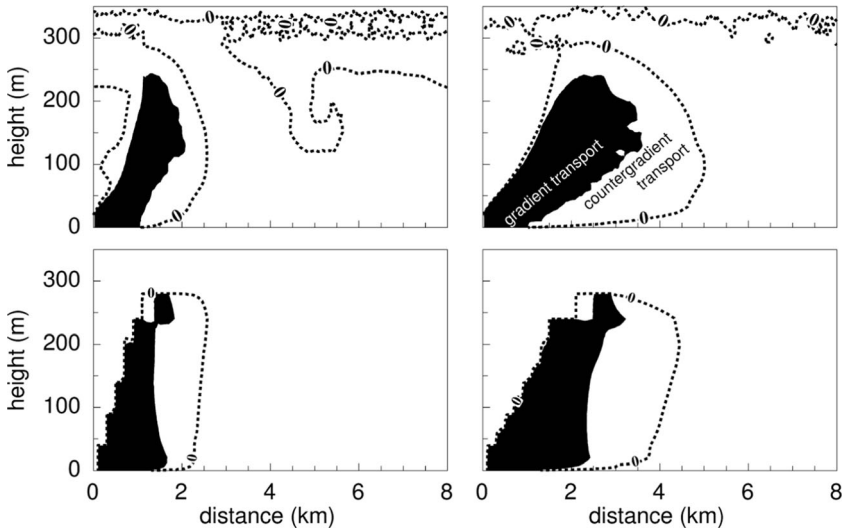

Fig. 11 The convective plume region over a lead (position between 0- and 1-km distance) is shown for two wind speeds (*left* $U = 3$ m/s, *right* $U = 5$ m/s) roughly as the region bounded by the 0-contour line. Also, regions with heat fluxes along the gradient of potential temperature (*black area*) and with countergradient fluxes (*white area* bounded by the 0-contour) are shown as modelled with the LES PALM (*top*) and with the mesoscale model METRAS (*bottom*). Figure from Lüpkes et al. (2008b)

show that the above parameterizations can be considered as a first step towards an adjustment of convection parameterizations to the grey zone in case of shallow convection over leads. Forthcoming climate models should account for the nonlinear dependence of fluxes on the sea ice concentration.

2.5.2 Cold-air outbreaks

Processes over leads can influence the inner polar ocean regions and the marginal sea ice zones, but during cold-air outbreaks (CAOs) energy fluxes of similar magnitude occur also over wide ocean regions with open water. Then, strong roll convection develops and the atmospheric boundary layer height increases from roughly 100 m over the polar marginal sea ice zone to 1–2 km in a far distance (Fig. 12). Several 100 km downstream of the ice edge, typically, a transition from roll to cellular convection takes place.

The patterns of organized convection, which are visible by cloud streets, are observed over Greenland and the Barents Sea in more than 50 % of the time during winter (Brümmer and Pohlmann 2000). Although similar statistics for the Antarctic are not yet available, satellite images show that CAOs with organized convection are a frequent phenomenon during off-ice flow, e.g. over the Bellingshausen Sea. Studies of CAOs in the Arctic can be considered as representative also for the Antarctic. Due to their impact on the exchange processes between ocean and atmosphere, it is important that they are well represented by parameterizations used in numerical weather and climate models.

Several studies (e.g. observational studies by Brümmer 1999; Hartmann et al. 1997) show that roll convection can substantially contribute to vertical transport of heat, moisture, and momentum. Therefore, it is often argued that vertical transport might be enhanced by rolls (e.g. Kristovich et al. 1999). However, as discussed in Gryschka et al. (2014), this needs to be proven. One reason is that it is not possible to find an observed reference case without rolls for the same large-scale forcing. A second reason is that, so far, it was assumed

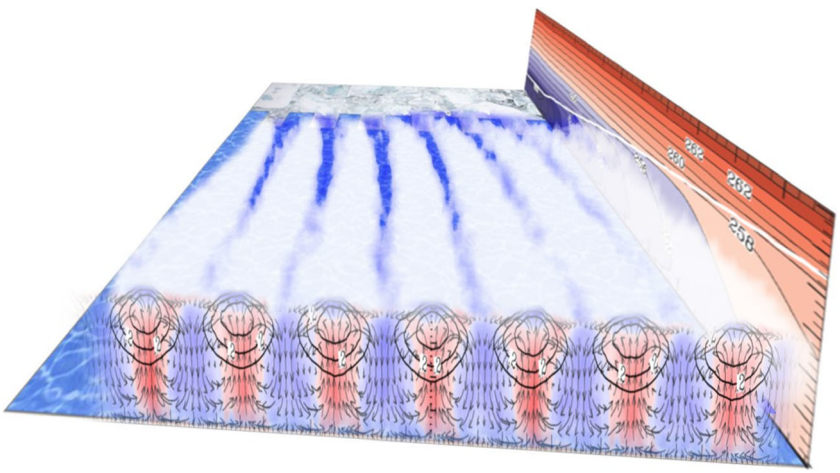

Fig. 12 Schematic figure of roll convection and cloud streets during a CAO derived from a PALM simulation. The cross section in the *front* shows the secondary circulation, the cross section on the *right* the time averaged potential temperature and the height of the CBL (*white line*)

that rolls in CAOs are developing by a pure self-organization mechanism so that again—for the same forcing—no case can exist without rolls. However, Gryschka et al. (2008) have shown with the LES model PALM (Maronga et al. 2015) that this assumption is not generally valid. They introduced and distinguished the terms 'forced roll convection' and 'free roll convection'. Free rolls develop by a pure self-organization of the flow only for small values of the stability parameter $-z_i/L$ (<10), where z_i is the height of the convective mixed layer and L is the Obukhov length. Forced rolls are triggered by upstream heterogeneities in the surface temperature (e.g. in the marginal ice zone in case of CAOs) and can develop also for much larger values of $-z_i/L$. Because in CAOs, $-z_i/L$ typically is much larger than 10 (e.g. in most of the observed CAOs in Brümmer (1999)), it can be expected that forced rolls are the dominant type of rolls within CAOs situations.

These findings allow a comparison of LES runs with and without rolls using the same large-scale meteorological forcing. This can be achieved by prescribing the surface temperatures with or without upstream heterogeneities as was done in the LES parameter study of Gryschka et al. (2014). The authors carried out 27 LES for 12 different CAO scenarios, covering a wide parameter range typical for CAOs. The stationary model domain was large enough to cover the development of the convective boundary layer (CBL) and roll convection for a wide distance over the ocean (up to 160 km from the sea ice edge), while the resolution of 50 m was fine enough to resolve small-scale unorganized turbulence. For each scenario, a roll and non-roll case was simulated and the wavelength of the rolls varied.

The main result of this study is, although rolls can contribute significantly to the total vertical turbulent fluxes, that these fluxes do not differ between roll and non roll-cases (Fig. 13; exemplary for the buoyancy and moisture fluxes for one CAO scenario). In other words, forced roll convection does not increase vertical transports but takes over part of the unorganized turbulent transport. Therefore, this study suggests that roll convection must not be treated by an additional parameterization scheme in numerical weather prediction and climate models. However, as mentioned above, in the future the resolution of weather prediction models will reach the grey zone, and (forced) roll convection might be explicitly resolved, leading to an overestimation of vertical fluxes (if parameterizations are not adapted).

There are also studies with mesoscale non-eddy resolving models (Wacker et al. 2005; Chechin et al. 2013)

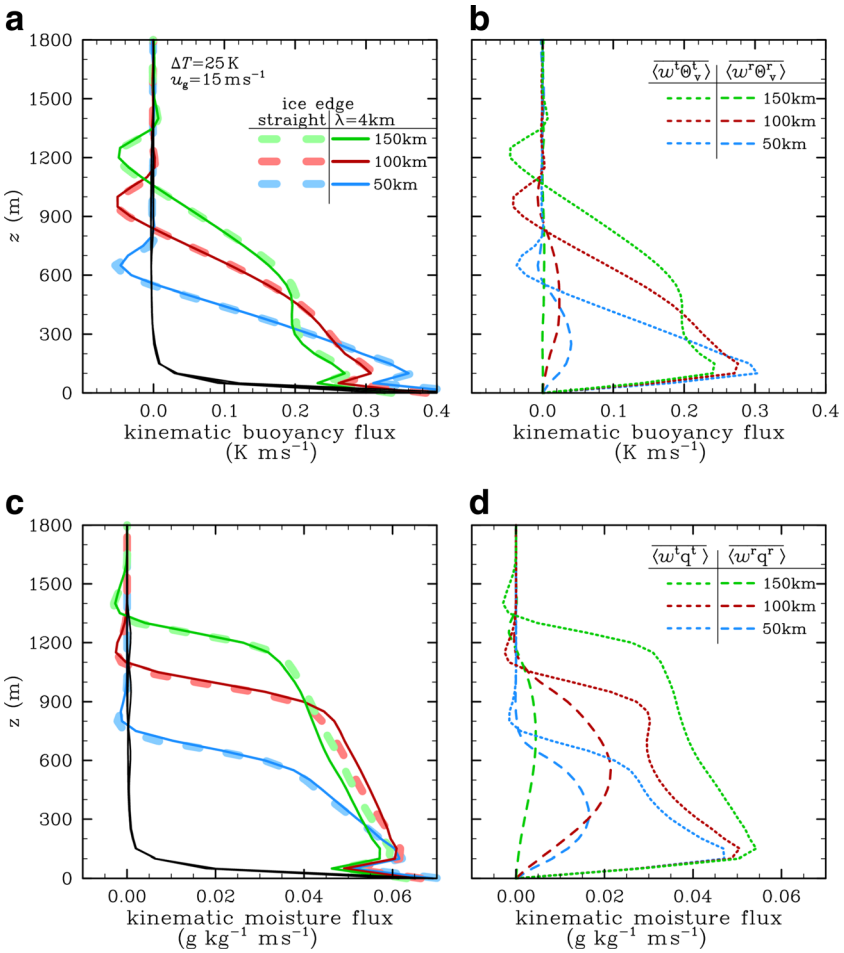

Fig. 13 Vertical profiles averaged over time and along y (mean ice edge orientation) of the kinematic buoyancy fluxes (**a**, **b**) after 17-h simulated time and the kinematic moisture fluxes (**c**, **d**) at successive distances from the ice edge for one CAO scenario. **a**, **c** The total turbulent fluxes for the roll (*solid lines*) and non-roll case (*dashed lines*) are shown. **b**, **d** The (resolved) contributions by rolls (*long dashed lines*) and unorganized turbulence (*short dashed lines*) for the roll-case are shown, respectively. The *solid black lines* (appearing as almost one line, **a**, **c**) represent the subgrid-scale contributions to the total turbulent fluxes. (*Spikes* in the profiles (*left column*) below 100 m appear only due to the analysis of fluxes in post processing and do not occur within the model physics (see Gryschka et al. (2014)). Figures from Gryschka et al. (2014)

which demonstrate that the observed development of the convective boundary layer during CAOs, including turbulent fluxes, are well reproduced with grid sizes of 4–15 km when adequate non-local turbulence closures are used. These closures do not need to account explicitly for roll convection, which can be explained by the findings of Gryschka et al. (2014) described above. Furthermore, Chechin et al. (2013) found that the formation of a wind maximum in the convective layer over open water with strong impact on the turbulent fluxes requires grid sizes smaller than 30 km for an accurate reproduction.

2.5.3 Katabatic wind and polynyas

The katabatic wind, developing on the Antarctic Ice Sheet, represents a key factor for the exchange of energy and momentum between the atmosphere and the underlying surface. Considering the large area of the Antarctic continent, this wind system plays also an important role in the global energy and momentum budget. A generally stable stratification over the ice slopes leads to the development of a katabatic wind system, which enhances air/snow interaction processes and influences the surface mass balance (van Lipzig et al. 2004; van de Berg et al. 2006). Wind speeds up to gale force are often observed in confluence zones and regions of steep topography near the Antarctic coast (Loewe 1972). A special point of interest is the modification of katabatically generated air flows when passing over the coastline and interacting with the sea ice or open water surface by forming or maintaining polynyas, which represent important areas of sea ice production and brine formation.

In the last two decades, a couple of numerical investigations of the katabatic wind system in Antarctica have been performed using 3D meso-scale models (e.g. Heinemann 1997; van Lipzig et al. 2004; Parish and Bromwich 2007; Dethloff et al. 2010). It was found that a high model resolution of at least 15 km is needed to capture the katabatic wind in regions near the coast or in topographically structured areas such as the Antarctic Peninsula.

In the framework of SPP 1158 mesoscale model simulations were conducted for the Weddell Sea using a high-resolution (5 km) limited-area non-hydrostatic atmospheric model (Ebner et al. 2014). In addition, a sea-ice/ocean model with enhanced horizontal resolution (3 km) was forced with the high-resolution data of the atmospheric model (Haid et al. 2015). The mean wind field for the winter 2008 is presented in Fig. 14. Over the large and flat Filchner-Ronne Ice Shelf (FRIS) and over the sea ice-covered Weddell Sea, wind speeds do not exceed 6 m s^{-1}. In the eastern Weddell Sea, areas with high wind speeds occur over the ice slopes towards the FRIS and in the area of Coats Land, where katabatic forcing is strong leading

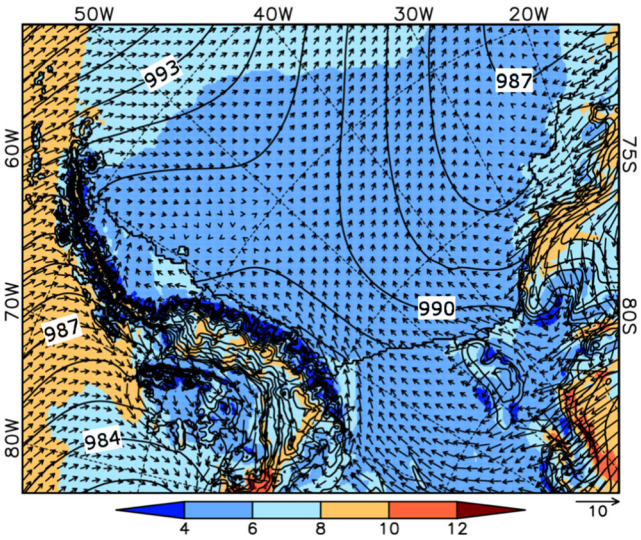

Fig. 14 Model domain with 5-km resolution and mean 10-m wind speed (colour-coded) in metres per second and mean 10 m vector wind (every eighth grid point) in metres per second for March to August 2008. Contour lines over sea ice/ocean show the mean sea level pressure (interval = 1 hPa). The *black polygon* marks the area of Coats Land/Luitpold Coast (from Ebner et al. 2014). Copyright Cambridge University Press, reprinted with permission

to intensified winds with high directional constancy. Enhanced offshore winds in the southeastern part of the Antarctic Peninsula indicate the presence of a barrier wind system.

Luitpold Coast is the only area in the Weddell Sea where katabatic winds pass the coastline and contribute to polynya formation. The analysis of time series for wind, polynya area, and forcing terms shows that changes in polynya area are mainly controlled by the downslope component of the surface wind (Fig. 15). The correlation between wind and changes in polynya area is 0.71 for the complete study period and 0.84 for July. The downslope surface offshore wind component of Coats Land is mainly

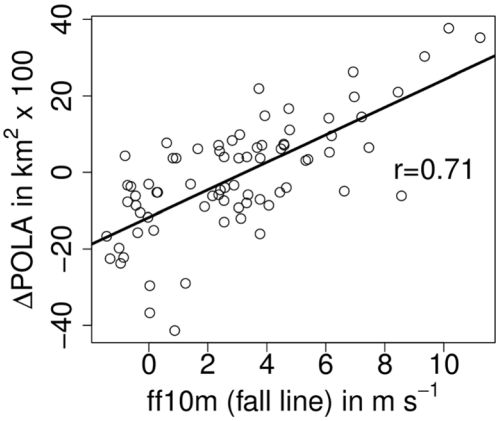

Fig. 15 Day-to-day change of large polynya area (POLA) changes and 10-m wind speed along the fall line for the Luitpold Coast area for winter 2008 (from Ebner et al. 2014). Copyright Cambridge University Press, reprinted with permission

steered by a pressure gradient due to katabatic force. Interestingly, the superimposed synoptic pressure gradient is opposed to the katabatic force during major katabatic wind events (Ebner et al. 2014).

The correct representation of the atmospheric forcing on polynya formation is crucial for the quantification of dense shelf water formation in the coastal polynyas of the Weddell Sea. Haid et al. (2015) found a large sensitivity of coastal polynya formation in the southwestern Weddell Sea to the atmospheric forcing for the sea ice-ocean model FESOM, using different coarse resolution global atmospheric analyses/reanalysis data and high-resolution COSMO model data. Major differences occur in mountainous areas where wind is strongly guided by surface topography. Particularly at Coats Land and along the Antarctic Peninsula, the use of high-resolution forcing results in a substantial improvement of the representation of polynya formation processes.

2.6 Sea ice production in Weddell Sea polynyas

Open water and thin sea ice areas, associated with wintertime polynyas in the coastal areas of the southern Weddell Sea, represent an enormous energy source for the atmosphere but also a large source of High-Salinity Shelf Water (HSSW), which plays a major role for the deep and bottom water formation and ocean circulation under the Filchner-Ronne Ice Shelf (Haid et al. 2015). HSSW production is directly related to sea ice production, which, therefore, is an important quantity in sea-ice/ocean modelling. However, direct measurements of sea ice production in the coastal polynyas are rare. This lack of in situ data is partly remedied by satellite-based studies. The majority of recent satellite studies of sea-ice production in Weddell Sea polynyas rely on passive-microwave sensors (Kern 2009; Drucker et al. 2011; Nihashi and Ohshima 2015). The main disadvantages of passive-microwave retrievals of sea ice production are the coarse resolution and the fact that thin-ice covered polynyas often remain undetected.

A long-term study for coastal polynyas in the southern Weddell Sea was conducted by using Moderate-Resolution Imaging Spectroradiometer (MODIS) thermal-infrared imagery. This allows for the determination of thin-ice thicknesses and sea-ice production on a daily basis with a high spatial resolution of 2 km (for details see Paul et al. 2015a,b). A continuous and cloud-cover corrected time series of polynya dynamics during the austral winter period (April to September) for the southern Weddell Sea for the period 2002–2014 was established. For a comparison with other models or satellite-based studies, the Weddell Sea was divided into sub-regions of potential polynya areas (Fig. 16). A special hot spot is the area around the grounded iceberg A-23A (IB), which is the result of a large calving event of the Filchner Ice Shelf in 1986. The iceberg has an area of about 3600 km^2 and is often neglected in sea ice-ocean models.

The most efficient sea ice production areas are off Ronne Ice Shelf (RO) and Brunt Ice Shelf (BR) (Fig. 17). The Antarctic Peninsula and Coats Land areas yield only relatively small contributions, while the surrounding of iceberg A-23A (IB) and Filchner Ice Shelf are of medium range. All regions show a high interannual variability and, except for Coats Land, a negative trend for sea ice production. On average over 13 years, the annual wintertime sea ice production amounts to 28 km^3 for the Ronne Ice Shelf, 28 km^3 for the Brunt Ice Shelf, 11 km^3 for iceberg A-23A, 9 km^3 for the Filchner Ice Shelf, 4 km^3 for the Antarctic Peninsula, and 4 km^3 for Coats Land. This shows that neglecting the presence of iceberg A-

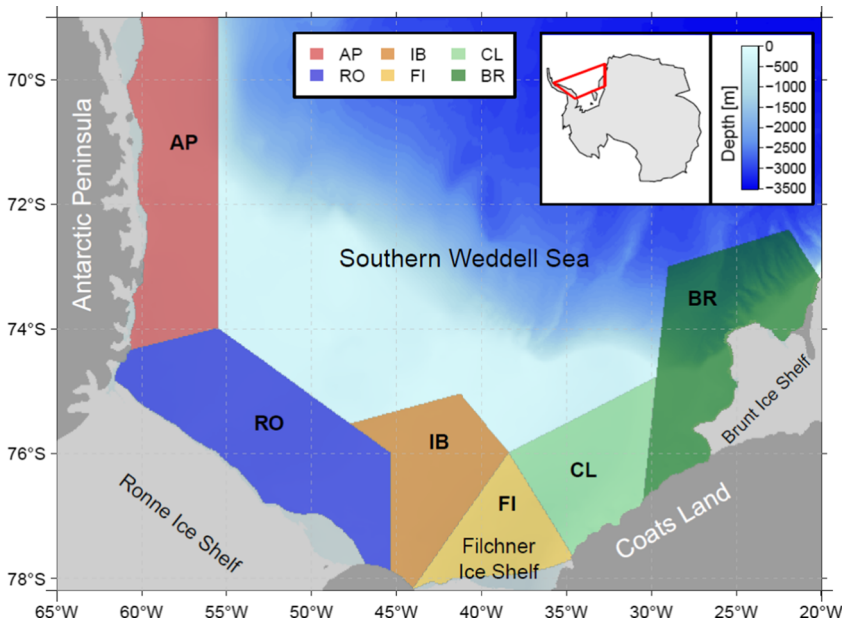

Fig. 16 Sketch of the study area in the southern Weddell Sea with sub-regions along the coast: Antarctic Peninsula (*AP*), Ronne Ice Shelf (*RO*), the area around the grounded iceberg A-23A (*IB*), Filchner Ice Shelf (*FI*), Coats Land (*CL*), and the Brunt Ice Shelf (*BR*). *Colour shadings* show the bathymetry based on Arndt (2013). From Paul et al. (2015b)

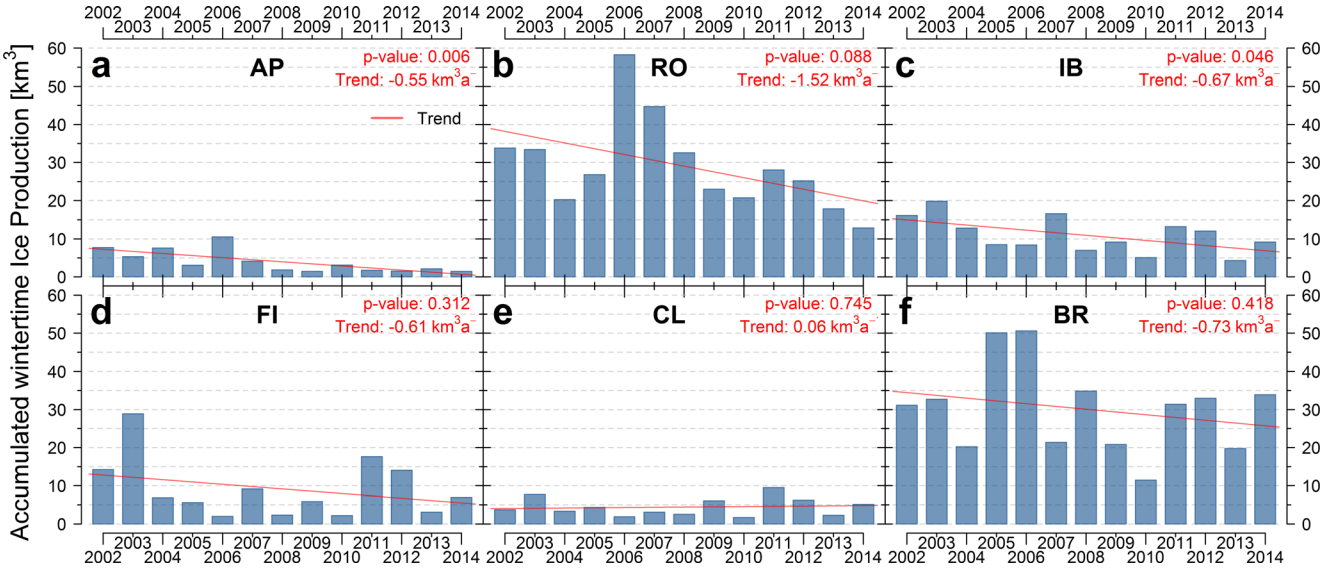

Fig. 17 Accumulated seasonal ice production [km^3, IP] for the years from 2002 to 2014 during the winter period from April to September. The *red line* indicates the multi-year regional trend in km^3/a. *p* value and numeric trend are stated in the *top right corner* for each sub-region (from Paul et al. 2015b)

23A would lead to a considerable underestimation of HSSW formation in the southern Weddell Sea.

The comparison of sea ice production between our study and other recent model or satellite-based studies in the southern Weddell Sea shows that our data yield generally lower sea ice production values; e.g. the model results of Haid and Timmermann (2013) for the Antarctic Peninsula are much higher. Drucker et al. (2011) found an average of 99 km^3 for the Ronne Ice Shelf, 112 km^3 for the Brunt Ice Shelf, and 30 km^3 for the region around the grounded iceberg A-23A. These estimates are three times higher than ours. There may be several reasons for these large differences: (i) Coarse resolution data like passive microwave tend to yield higher sea ice production rates (Nihashi and Ohshima 2015). (ii) Differences exist in the parameterization of turbulent and radiative atmospheric fluxes of different methods, e.g. if the transfer coefficients are not stability dependent. (iii) The atmospheric data driving the thin-ice retrieval has a large impact on the ice production, particularly if there is a cold bias as it is known for National Centres for Environmental Prediction (NCEP) reanalyses products (Lindsay et al. 2014). Since we are using state-of-the-art parameterizations (Adams et al. 2013) and ERA-Interim reanalysis data, we think that our high-resolution (2 km) data set represents a new benchmark for the comparison with model estimates of sea ice production in Weddell Sea polynyas.

3 Changes in the Southern Ocean and its reverberation in cryosphere and biosphere

Changes in the Southern Ocean significantly influence global climate in many ways and on a large range of time scales. The capacity of the ocean to store heat and carbon is a prerequisite to understand the strength of the fluctuations in global atmospheric temperature and CO_2 during the last several 100,000 years. The Southern Ocean is a key region for the exchange of energy and gases between atmosphere and the deep ocean. Here, surface water is converted to deep and bottom water and the deepest branch of the global meridional overturning is formed. Compared to other ocean basins, the warming rate in the Southern Ocean is the highest. Interaction of relative warm water with ice sheets is thought to be one of the major processes causing sea level rise and ice sheet mass loss; today, about 20 % of the global sea level rise is already attributed to this process. Warming of the Southern Ocean might also influence the formation rates of deep and bottom water as well as the uptake of anthropogenic CO_2. Another peculiarity of the Southern Ocean is the dominant role of iron availability for the control of biological carbon fixation and the interaction with processes involving microorganisms on the transformation and transport from surface waters to sediments. Even though chemical and biological interactions affect and interconnect the biogeochemical cycles of carbon and trace elements of the Southern Ocean, so far, few studies have addressed this complex research area.

In the last decades, research in the Southern Ocean contributed to new insights into the interaction between ocean and ice sheets, the changes in water mass characteristics, ventilation, and formation rates and associated storage of anthropogenic carbon as well as into the cycling of carbon, nutrients, and trace metals. Most oceanic field studies have been conducted in the Atlantic sector of the Southern Ocean, especially in the Weddell Sea. Here, ocean water has access to two large ice shelves, the Filchner-Ronne Ice Shelf (FRIS) and the Larsen Ice Shelf (LIS). Interaction between the ocean and these ice

shelves is crucial for the formation of Weddell Sea Deep Water (WSDW) and Weddell Sea Bottom Water (WSBW), the main precursors for Antarctic Bottom Water (AABW), which forms the deepest limb of the global, climate-relevant meridional overturning circulation. However, the importance, local variability, and evolution of deep and bottom water formation under changing climate conditions as a long-term sink for atmospheric anthropogenic carbon (C_{ant}) is still under debate, particularly in the Weddell Sea.

3.1 Freshwater input through ice shelf basal melting

In a steady state world, the snow accumulation on top of the (up to 4000-m thick) Antarctic Ice sheet (Section 2.4) is balanced by the transfer of mass to the ocean, either by iceberg calving at ice shelf fronts or by melting of ice shelf bases (Jacobs et al. 1992). Recent studies, based on remote sensing, have revealed that both transfer processes are of equal relevance, and the basal mass loss in the Weddell Sea was found to be 118 ± 52 Gt year^{-1} (Depoorter et al. 2013). Independent evidence comes from earlier estimates of Huhn et al. (2008), who used the distribution of He and Ne isotopes to infer the contribution of basal melt to the Weddell Sea water masses. Combined with their estimates of the formation rates of deep and bottom water they reported 35 ± 19 Gt year^{-1} for LIS and 123 ± 53 Gt year^{-1} for FRIS.

As a result of the interaction between ocean and ice shelf (Figs. 18 and 19), a relatively fresh melt-water plume leaves the ice shelf cavity and either contributes to the formation of deep and bottom water at the continental shelf break and slope (Foldvik et al. 2004; Rodehacke et al. 2007; Huhn et al. 2008) or influences the stability of the water column in front of the ice shelf or further downstream on remote continental shelves (Hellmer 2004). A more stable shelf water column hampers deep convection that brings (i) ocean heat to the surface, reducing sea ice formation rates, and (ii) cold, saline surface water to the sea floor, contributing to dense water formation and basal melting (Fig. 18).

This self-regulating process can only be bypassed if the heat for melting is provided by the open ocean. Such situation is known for the Amundsen and Bellingshausen Seas, where at mid-depths Circumpolar Deep Water (CDW), originating from the Antarctic Circumpolar Current (ACC), penetrates onto the continental shelf and cascades down towards the ice shelves draining the West Antarctic Ice Sheet (Nakayama et al. 2013). This heat supply causes the highest basal melt rates so far known in Antarctica with estimates reaching up to 100 m per year underneath the Pine Island Glacier Ice Shelf (Dutrieux et al. 2014). The resulting freshwater plume primarily influences the surface layer but can also be mixed into the CDW due to convection in front of the ice shelf, thus reducing the heat content of the inflowing warmer deep water. One might speculate that the large volume of glacially derived freshwater is one of the reasons for the Amundsen and Bellingshausen Seas not being a site for deep and bottom water formation today. Part of the meltwater injected into Amundsen Sea is advected northward and into the ACC (Kusahara and Hasumi 2014) while the other part is transported with the coastal current into the Ross Sea. Here, according to a numerical study (Nakayama et al. 2014), the meltwater is likely to be responsible for the observed long-term decrease of shelf water salinity (Jacobs et al. 2002). The freshening in the Ross Sea, in turn, is suggested to have caused the decline in the salinity of the AABW in the Australian Antarctic Basin (Rintoul 2007). The latter demonstrates the intricate transfer of surface signals, due to changes in the mass balance of the Antarctic Ice Sheet, into the deep ocean.

In the large embayments, such as the Weddell and Ross Sea, the circulation in the large sub-ice shelf cavities is driven by HSSW (Fig. 19) formed in polynyas and leads (see Section 2.6) near the ice shelf fronts (Tamura et al. 2008; Haid and

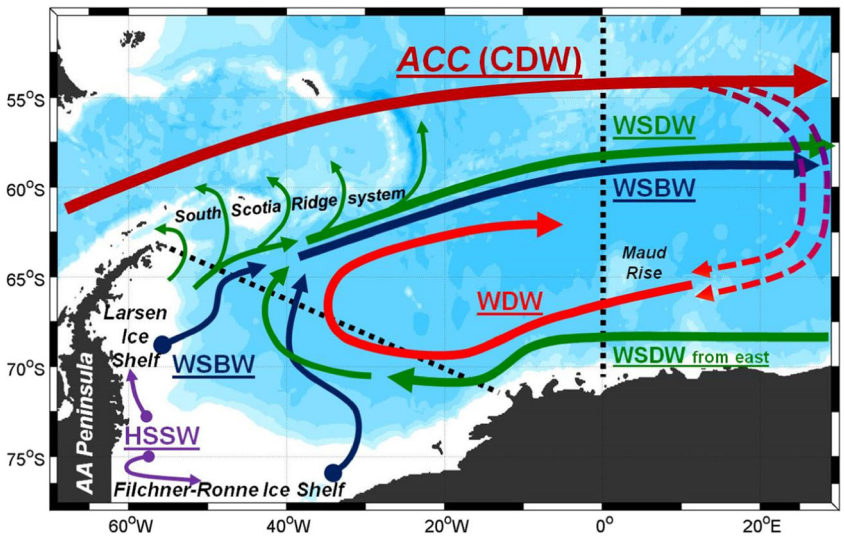

Fig. 18 Map of the Atlantic sector of the Southern Ocean south of the Subpolar Front. Deep water masses and schematic circulation are indicated by *arrows*. *ACC* Antarctic Circumpolar Current, *CDW* Circumpolar Deep Water; *HSSW* High-Saline Shelf Water, *WSDW* Weddell Sea Deep Water, *WSBW* Weddell Sea Bottom Water. Black stippled: the two repeat sections: the Prime Meridian and the Weddell Sea section

Timmermann 2013). Although at surface freezing temperature, HSSW fuels area-mean basal melt rates of a few decimetres per year (several meters per year locally along the deep grounding lines) due to the pressure dependence of the freezing point. The resulting meltwater plume is super-cooled, i.e. below the in situ surface freezing point, and less buoyant than the ambient shelf water, thus following the bottom bathymetry on its way to the continental shelf break (Fig. 19). In the southern Weddell Sea, the freshwater of glacial origin predominantly gets incorporated into the WSBW that is confined to the deep Weddell Basin. Basal melt water that is more directly fed into the World Ocean originates from the LIS fringing the western Weddell Sea (Huhn et al. 2008). Part of the LIS freshwater remains on the northwestern Weddell Sea continental shelf; the observed freshening of the winter shelf water column near the tip of the Antarctic Peninsula (Hellmer et al. 2011) as well as the salinity decrease of the deep waters in the central basin of Bransfield Strait (Garcia and Mata 2005) might have been caused by an increase of LIS basal melting.

The present conditions in the southern Weddell Sea might change in the near future. According to IPCC-scenario simulations with two coupled ice-ocean circulation models of different architecture, forced with the atmospheric output of the climate model HadCM3, changes in atmospheric temperature, the wind field, sea ice cover, and the density structure on the continental shelf may allow the slope current to penetrate into the Filchner Trough (Hellmer et al. 2012). This current transports Warm Deep Water (WDW), a derivative of CDW, into the inner Weddell Sea. Within a decade, the bottom temperatures increase by 2 °C all the way from the continental shelf break to the grounding line of FRIS, boosting the basal mass loss by roughly a factor of 10 during the first 150 years of simulation (Fig. 20, Timmermann and Hellmer 2013). The associated thickness decrease has severe consequences for the buttressing potential of the ice shelf and the dynamics of the ice streams mainly draining East Antarctica (Thoma et al. 2015). The increase in glacial meltwater additionally freshens the southern Weddell Sea continental shelf, contributing to a further decline of the shelf water density. This positive feedback mechanism might only come to a hold once the freshwater input due to basal melting is stopped either by atmospheric conditions forcing the slope current back into the open ocean or by a severe size reduction of the ice shelf.

For LIS, however, the basal mass loss does not change much over the next centuries; it even decreases in the twenty-second century (Fig. 20, Timmermann and Hellmer 2013). The main reason is the presence of cold, fresh meltwater from FRIS that prevents WDW intrusions at LIS. As demonstrated for the Amundsen and Ross Seas (Nakayama et al. 2014), this indicates again a link between the different ice shelves via the continental shelf and slope circulations and calls for circumpolar rather than regional approaches if the interaction of the Southern Ocean with Antarctic ice shelves is investigated.

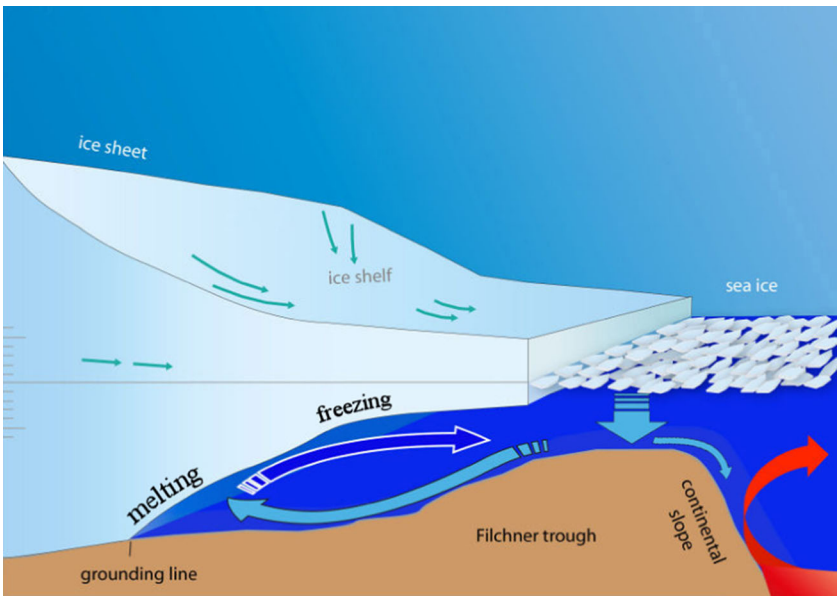

Fig. 19 Schematic of today's circulation in the southern Weddell Sea including the continental shelf and the sub-ice shelf cavity. The slope current transports warm deep water (*red arrow*) which stays off the continental shelf. Sea ice formation in front of the ice shelf produces dense shelf water (*thick blue arrow*), that either sinks down the continental slope or follows the bottom topography into the ice shelf cavity. Due to the pressure dependence of the freezing point, the cold water is able to melt several meters per year of ice at the deep grounding line. The resulting freshwater plume rises along the ice shelf base. Depending on the temperature of the inflowing water and the length of the ice shelf, the plume might become in situ super-cooled, favouring ice crystal formation in the water column and the accumulation of a marine ice body at the ice shelf base

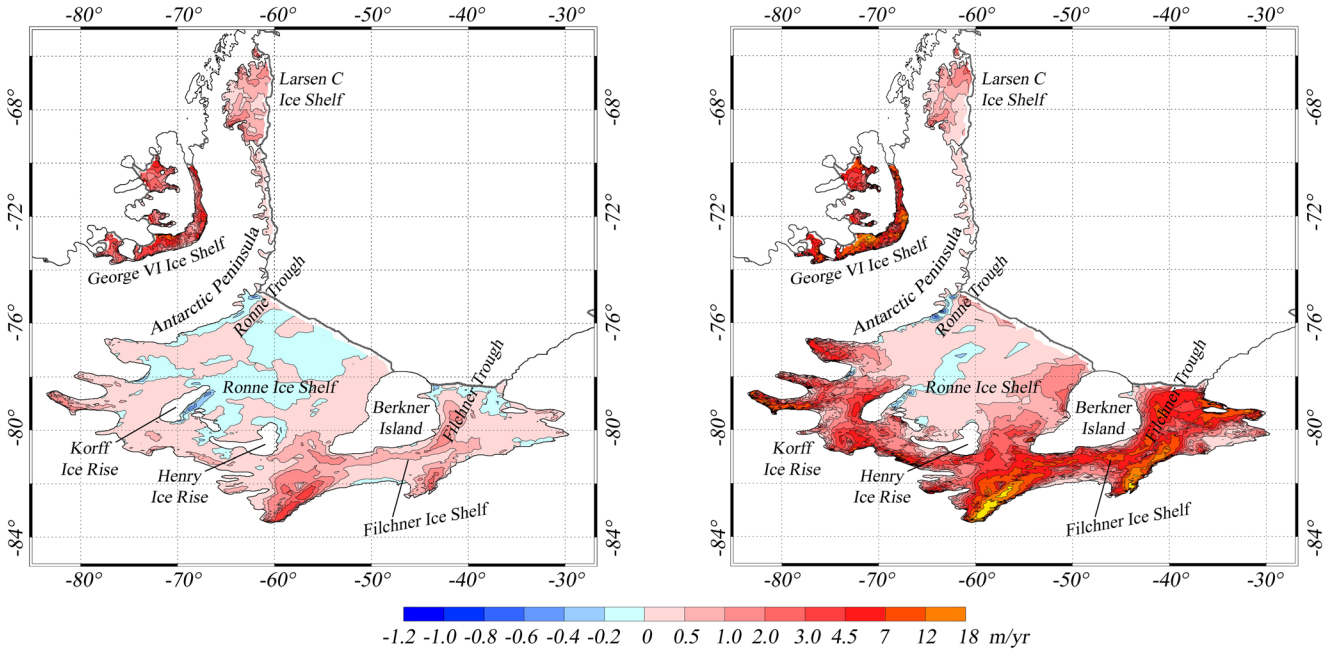

Fig. 20 Basal melt rates (m year^{-1}) for the Filchner-Ronne (FRIS), Larsen C (LIS), and George VI ice shelves for (*left*) present-day conditions (10-year average 1990–1999) and (*right*) in the middle of the twenty-second century (projection for 2140–2149 mean) in a FESOM simulation forced with HadCM3 data for the IPCC's A1B scenario. Note the non-linear colour scale. (after Timmermann and Hellmer, 2013)

3.2 Water mass and ventilation changes in the Weddell Sea

The only pathway by which the interior Weddell Sea gains significant amounts of heat is the inflow of warm (>1.3 °C) and saline CDW of the ACC (Fig. 18) with the southward oriented eastern limb of the Weddell Gyre between 20° E and 30° E (Schröder and Fahrbach 1999). When CDW enters the Weddell Sea proper across the Prime Meridian its warm core occupies the depth range between 150 and 600 m. The inflow is split into two branches, one centred between 63° S and 64° S associated with the topographic slope north of Maud Rise and the other between 68° S and 69° S associated with the continental slope of Antarctica (Cisewski et al. 2011). Downstream of Maud Rise the two cores mix mainly isopycnically (Leach et al. 2011) to form the so-called Warm Deep Water in the Weddell Sea. CDW is predominately fed by the North Atlantic Deep Water but also contains deep waters from other ocean sources.

Starting in 1984, the monitoring of a high-resolution hydrographic section along the Prime Meridian (e.g. Fahrbach et al. 2004, 2011) represents the longest time series in the Southern Ocean (Fig. 21). Together with the section across the Weddell Sea from Kap Norvegia to Joinville Island at the tip of the Antarctic Peninsula (Fahrbach et al. 2004), it constitutes the major part of the hydrographic data from the Atlantic sector of the Southern Ocean. Global ocean temperature analysis (Purkey and Johnson 2010) showed that warming from the 1980s to the 2000s was stronger south of the Subantarctic Front of the ACC than in the global ocean below 1000-m depth on average. In approximately the same time period, between 1984 and 2008, WDW temperature variations in the order of 0.06 °C were observed (Fig. 21), with a positive trend of 0.04 °C (Fahrbach et al. 2011). Whether the observed WDW warming at the Prime Meridian is related to the mean warming of the ACC south of the Subantarctic Front (Rhein et al. 2013) or to variations in the advection of CDW by the two branches and their subsequent mixing to form the WDW, cannot be resolved with the existing data. Testing the utility of available ocean reanalysis products in yielding model results that reproduce the existing observations from the Weddell Sea unfortunately also revealed limited capabilities of the model reanalyses (Dotto et al. 2014).

WDW takes a crucial role in the ocean-ice shelf interaction, hence basal melting, and in the formation of deep and bottom water in the Weddell Sea, the major source (about 60 %, Orsi et al. 1999) of AABW. One of the important predecessors of AABW is WSBW. It results from the interaction of HSSW, locally formed during sea ice formation (Foster and Carmack 1976) in front of FRIS and LIS (Foldvik et al. 1985; Weppernig et al. 1996; Foldvik et al. 2004; Huhn et al. 2008), and the mixing with WDW. Further entrainment of WDW forms WSDW found above the WSBW. Additionally, deep water from easterly sources with comparable properties as WSDW enters the Weddell Basin in the deep southern boundary current, probably formed off Cape Darnley west of Prydz Bay (Mantisi et al. 1991; Hoppema et al. 2001; Klatt et al. 2002; Lo Monaco et al. 2005; Oshima et al. 2013). The shallower fractions of WSBW and WSDW exit the

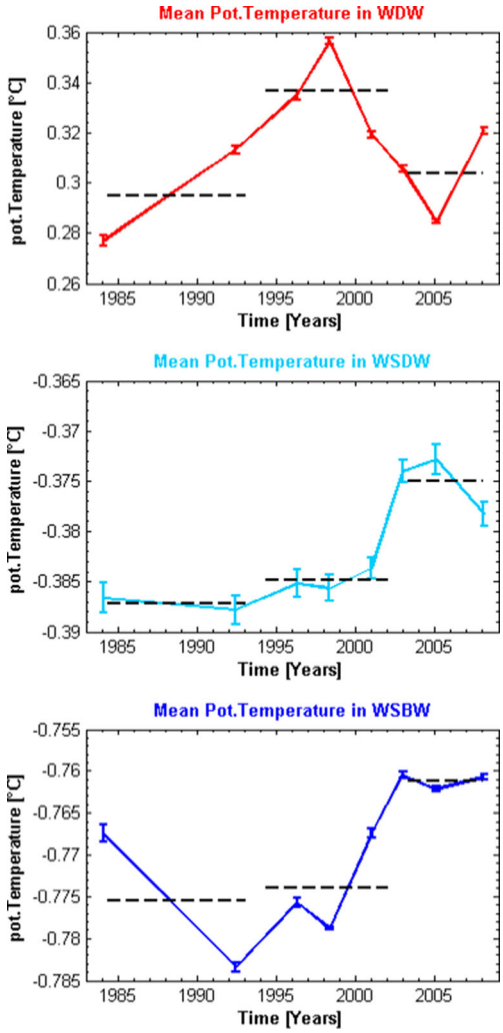

Fig. 21 Temporal changes of the section mean potential temperature (°C) in the Weddell Gyre from 1984 to 2008 observed along the Prime Meridian between 56° S and the Antarctic continent. Water mass boundaries are defined by neutral density surfaces for Warm Deep Water (*top*), Weddell Sea Deep Water (*middle*), and Weddell Sea Bottom Water (*bottom panel*). The *error bars* were calculated as the error of the mean value of independent samples. The time series are divided into three segments from 1984 to 1993, 1994 to 2002, and 2003 to 2008 for which the mean values are indicated by the *dashed lines*. Redrawn after Fahrbach et al. (2011)

Weddell Basin through gaps in the South Scotia Ridge (Muench et al. 1990; Whitworth et al. 1994; Gordon et al. 2001; Naveira Garabato et al. 2002; Schröder et al. 2002; van Caspel et al. 2015), underride the ACC, and power the lower limb of the meridional overturning circulation. Deeper fractions of WSBW and WSDW that do not spill over the South Scotia Ridge follow the Weddell Gyre circulation eastward (Fig. 18).

From transient tracer data taken between 1984 and 1995, Orsi et al. (1999, 2002) estimated a total AABW formation rate of 8.1 ± 2.6 Sv (1 Sv = 10^6 m^3/s), with AABW defined by neutral densities $\gamma^n > 28.27$ kg/m^3. In contrast, Broecker et al. (1997) using radiocarbon (^{14}C) and nutrient observations deduced a total AABW (here defined as 'ventilated water', deeper than 1000 m and silicate >90 μmol/kg) formation rate of 15 Sv. The discrepancy is thought to be caused by a reduction of AABW formation in more recent decades (see also Broecker et al. 1999).

The AABW formation rate in the Weddell Sea of 4.9 Sv determined by Orsi et al. (1999) is compatible with results inferred from current meter observations (3–4 Sv, Fahrbach et al. 1991), inverse modelling approaches (5–6 Sv, Sloyan and Rintoul 2001; Lumpkin and Speer 2007), and other hydrography or tracer-based estimates (4–5 Sv, Gordon et al. 1993; Gordon 1998; Mensch et al. 1998; Huhn et al. 2008). Recently, indications for changing water mass properties and a possible reduction of deep and bottom ventilation in the Weddell Sea have emerged. Hellmer et al. (2011) observed a substantial freshening of shelf water masses in the northwestern Weddell Sea, with possible implications for the subsequent bottom water formation. Conductivity-temperature-depth (CTD) sections from 1984 to 2008 revealed a significant warming in the deep water masses (Fig. 21), while WSDW became saltier and WSBW fresher (Fahrbach et al. 2011). Moreover, the cross section area occupied by WSBW at the Prime Meridian declined by 25 %. Purkey and Johnson (2012) estimated a reduction of WSBW in the Weddell Basin of roughly 3 Sv between the 1980s and 2000s. Based on long-term CFC time series, all deep water masses within the Weddell Sea have been continually growing older and less ventilated during the last 27 years. The decline of the ventilation rate of WSDW and WSBW by 18–23 % seems to be mainly caused by mixing with WDW, which aged much faster by 35 %. Increased entrainment of WDW into WSBW and WSDW or a deceleration of the Weddell Gyre circulation may also play a role. The Weddell Sea is not the only region where ageing of water masses was observed. Waugh et al. (2013) estimated that CDW aged in all Southern Ocean sectors between 30 and 60 % in the period of the early 1990s to the late 2000s (~60 % in the Atlantic sector) and attributed this age increase or ventilation decrease to an intensified westerly wind field over the ACC. A new concept of validity areas for tracer couples may help to identify and validate future changes in ventilation in these regions (Stöven et al. 2015).

Due to the involvement of surface water in the formation process, the WSBW and subsequently the AABW carry relatively high loads of atmospheric gases such as oxygen, transient tracers like the anthropogenic CFCs and C_{ant}, and therefore contribute to the ventilation of the global abyss. Despite their relevance, the variability of ventilation and formation rates of deep and bottom water and the related storage of C_{ant} in the Southern Ocean is currently not well constrained (e.g. Bullister et al. 2013). Classical oceanographic measurements (e.g. Fahrbach et al. 2011) combined with observations of helium and neon isotopes (e.g. Schlosser et al. 1990; Huhn

et al. 2008) and CFCs (e.g. Orsi et al. 1999; Klatt et al. 2002; Huhn et al. 2013) provided insight into the relevant physical processes. Numerical models with very high resolution are promising and necessary to account for the complex atmosphere-ocean-sea ice-interaction and for irregularities in the bottom topography. The latter influences the exchange of WDW across the continental shelf break as well as the processes under the ice shelf (Timmermann et al. 2012).

3.3 Changes in storage of anthropogenic CO_2 in the Southern Ocean: the Weddell Sea

Due to the transfer of near-surface water to greater depths, the global ocean absorbs and stores a significant fraction of C_{ant} emissions, namely about 155 ± 20 % Pg C [1 Pg C = 10^{15} g of carbon] until 2011, or one third of the total anthropogenic CO_2 emissions (e.g. Rhein et al. 2013). Large-scale estimates suggest that the Southern Ocean is a disproportional contributor to this uptake of C_{ant}; the share may be 40 % (Khatiwala et al. 2009). In the first place, uptake of anthropogenic CO_2 occurs at the sea surface forced by the continually rising atmospheric CO_2 content (due to fossil fuel burning), which causes steady CO_2 undersaturation at the air-sea interface. Data of Takahashi et al. (2009) evince the Southern Ocean surface layer tracking the atmospheric partial pressure of CO_2 (pCO_2) closely. Most C_{ant} is contained in the upper 400–500 m, distributed by wind-driven turbulent mixing in the surface layer and additional downward diffusion. North of the Polar Front, where water mass subduction occurs, the C_{ant}-charged water is sequestered in the Antarctic Intermediate Water (AAIW) and in the Subantarctic Mode Water (SAMW) and transferred equatorwards (Fig. 22a). Here, the majority of Southern Ocean C_{ant} is stored. South of the Polar Front, the surface water similarly takes up C_{ant}. However, two factors impede the full-fledged equilibration with C_{ant} from the atmosphere. First, sea ice, which occurs part—and in some regions most—of the year caps the ocean; and second, the large-scale upwelling of CO_2-rich, but C_{ant}-poor subsurface water into the surface layer. In the gyres south of the ACC, the divergent circulation causes particularly strong upwelling and, thus, a dilution of the C_{ant} signal.

Sequestration of C_{ant} south of the Polar Front mainly occurs via formation of dense deep and bottom waters. As mentioned before, C_{ant} is introduced into the WSBW via its surface water ingredients. Although frequent sea-ice cover might impede the uptake of C_{ant} by the shelf waters, significant amounts of C_{ant} have been observed in the subsurface Weddell Sea (Poisson and Chen 1987; Anderson et al. 1991; Hauck et al. 2010; Huhn et al. 2013). On the Prime Meridian, repeat section data covering the period 1973–2010 (Fig. 23) showed an increase of CO_2 of 1.2–1.4 ± 0.6 μmol kg^{-1} $decade^{-1}$ in the WSBW (Van Heuven et al. 2014). This increase significantly correlates with increases of the purely anthropogenic CFC-12, indicating that the C_{ant} increase is of genuine anthropogenic origin (Van Heuven et al. 2011). The CO_2 increase in the WSBW coincides with a remarkable decrease of dissolved oxygen and an increase in silicate (Van Heuven et al. 2014), which matches with potential temperature and salinity changes (Fahrbach et al. 2011). However, the C_{ant} increase in WSDW and WSBW is smaller than one would expect from the rising atmospheric CO_2 concentrations under a steady state ocean (Huhn et al. 2013). The observed decrease in the ventilation rate of the deep and bottom water masses in the Weddell Sea (Huhn et al. 2013) and the ACC (Waugh et al. 2013) affect C_{ant} and indicates that the latter assumption might not hold. C_{ant} uptake and storage slowed down by 14–21 % as compared to the steady-state situation with level ventilation. Besides the entrainment of WDW, which aged much stronger than the deep and bottom waters, the mechanism behind the reduction of C_{ant} uptake in the Weddell Sea may well be an elevated upwelling of subsurface water, which was shown at least during the 1990s and 2000s (Hoppema et al. 2015). This further reduces the C_{ant} concentration in the surface water by dilution with C_{ant}-poor water.

A decrease of the CO_2 uptake since the 1980s was also suggested by some large-scale data-based studies (e.g. Le Quéré et al. 2007). Changes in the Southern Annular Mode intensified the westerly winds and shifted their tracks southwards with the consequence of elevated upwelling of subsurface water enriched in (natural) CO_2. However, recently, the uptake of CO_2 in the Southern Ocean appears to have been increasing again (Landschützer et al. 2015). A more asymmetric atmospheric circulation around Antarctica may be causing this, possibly regulated by the La Nina conditions in the tropical Pacific (Landschützer et al. 2015). With a certain time lag, more C_{ant} will also be transferred into the deeper water masses and, thus, changing future trends should be expected there. These alleged climate changes are much debated and continuing research is necessary.

In the future, SAM-related climate changes are thought to continue (Thompson et al. 2011). Thus, the upwelling of subsurface water (like CDW or WDW) will also continue at an enhanced rate, and the rise of the C_{ant} concentration in the Weddell Sea surface layer will further be reduced in spite of the incessant C_{ant} undersaturation. On longer time scales (decades to centuries), the C_{ant} content of the CDW and thus of WDW will increase due to the invasion of C_{ant} in the source regions of the CDW; in addition, upwelling of CDW would transport C_{ant} to the surface layer of the Weddell Sea. This contemplation as yet excludes possible changes in the sea ice cover. Due to increased global warming, sea ice-free periods might get longer, thus enforcing the exchange of CO_2 with the atmosphere. The changes occurring in the Weddell Sea cannot be regarded as isolated, since upwelling is always

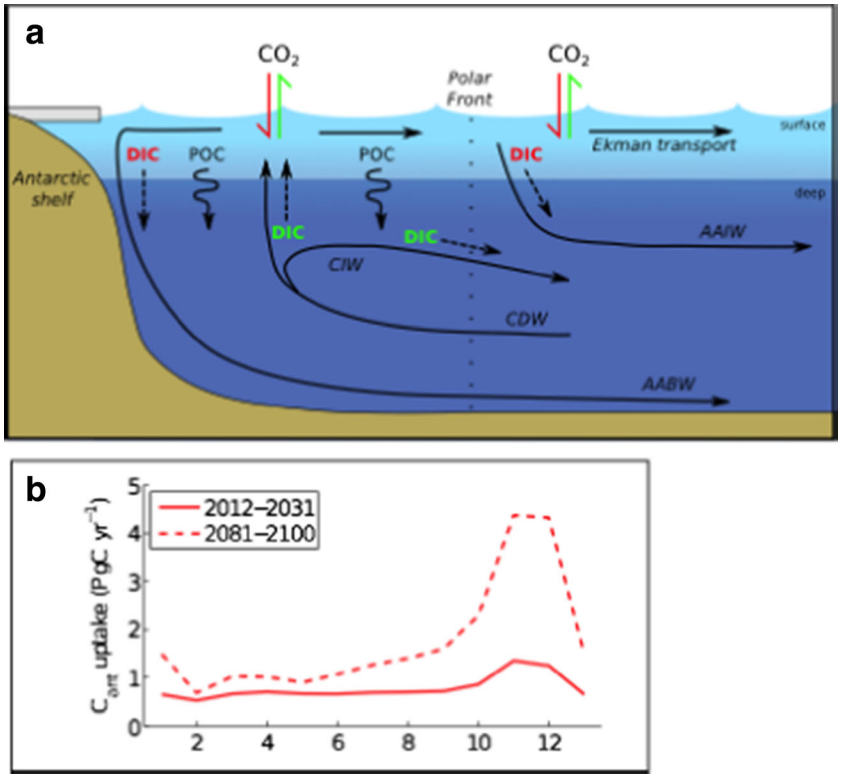

Fig. 22 **a** Scheme of the Southern Ocean circulation and the contemporary carbon cycle. *Dashed arrows* denote transport of natural (*green*) and anthropogenic (*red*) carbon due to advection and the solubility pump. Wiggled arrows indicate carbon fluxes by virtue of the biological carbon pump. *POC* particulate organic carbon, *DIC* dissolved inorganic carbon, *AAIW* Antarctic Intermediate Water, *CIW* Central Intermediate Water, is upwelled, *CDW* Circumpolar Deep Water, *AABW* Antarctic Bottom Water. Weddell Sea Bottom Water as mentioned in the text is one of the predecessors of AABW. Figure slightly modified after Hauck (2013). **b** Seasonal cycle of anthropogenic carbon uptake south of 44° S, at present (*solid line*, average over years 2012–2031) and at the end of the century (*dashed line*, 2081–2100). January is shown as the first and the last month of the seasonal cycle. Data from a model simulation as in Hauck and Völker (2015)

compensated by enhanced downwelling in other regions. Waugh et al. (2013) suggested that this will occur in northern regions of the ACC where mode waters are formed. This counteracting process was shown to occur in models (Hauck et al. 2013b) and represents a negative feedback for decreasing C_{ant} uptake.

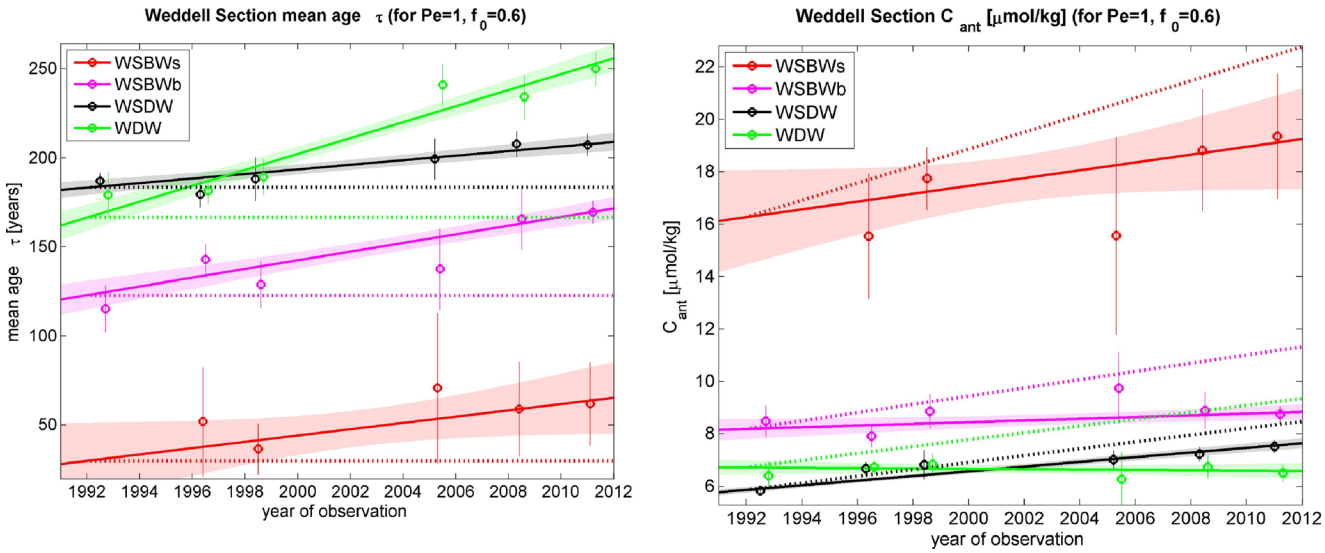

Fig. 23 Time series of ages in WDW, WSDW, and WSBW (*left*) and C_{ant} at the Weddell Sea section (location see Fig. 18). The *stippled lines* show the expected trends in these water masses when assuming a steady state ocean. The age of a water mass would remain constant, and the C_{ant} increase with time would only depend on the atmospheric concentrations. Updated from Huhn et al. (2013)

At present, uptake of C_{ant} occurs year-round at a relatively constant rate as it is mainly driven by the increase in atmospheric pCO_2. However, there is a strong seasonality of (natural) CO_2 uptake, with the largest part occurring in summer during phytoplankton blooms. In the future, the same level of biological production will lead to a larger uptake of CO_2 because the carbonate system will be less well buffered at higher Revelle factors, which then will be predominating (Hauck and Völker 2015). Most C_{ant} uptake will occur in austral spring and summer (Fig. 22b), due to the increased importance of the biological carbon pump with rising atmospheric CO_2.

In addition to the sequestration of inorganic carbon via the thermohaline advection, the downwelling of dissolved organic matter (DOM) also contributes to the vertical carbon flux in the ocean (Carlson et al. 2010). Marine dissolved organic carbon (DOC) forms a large reservoir in the global carbon cycle (662 Pg C, Hansell 2013), ~90 % of which is not bioavailable and chemically unreactive (refractory). Based on DOC concentration gradients, an export flux of ~86 Tg C $year^{-1}$ was calculated for the deep Atlantic (Hansell et al. 2009). Since the ultimate source of marine DOC is primary production and therefore CO_2, this export also contributes in parts to C_{ant} sequestration. Although the extent of this flux is 2–3 orders of magnitude smaller than the inorganic carbon pump, the residence time for refractory DOC is much longer than for inorganic carbon: DOC in the Weddell Sea and Southern Ocean has an average ^{14}C age of ~5500 years and deviates from the general global correlation of DOC concentration and age (Lechtenfeld et al. 2014; Druffel and Bauer, 2000). Individual organic fractions can reside for much longer-time scales than the average DOC (>24,000 year; Lechtenfeld et al. 2014).

The microbial process, which forms unreactive DOM is critical for an efficient sequestration of DOC: Incubation experiments demonstrated that surface bacteria in the Weddell Sea produce 5–9 % of non-labile DOC from simple organic substrates (Koch et al. 2014). Thus, DOC downwelling in the Weddell Sea contributes to the buffer in the ocean carbon cycle. It is not clear how this carbon buffer will evolve in the future global biogeochemical cycle and how it affects the climate system (Denman et al. 2007). Further removal of DOC depends primarily on microbial degradation and light availability (photo degradation). It was suggested that during the Eocene, a stratified and anaerobic ocean stored large amounts of DOC, which was quickly released after circulation restarted and ventilated the ocean, resulting in a rapid global warming event (Sexton et al. 2011). Although we know that DOC mineralization primarily depends on the molecular chemical composition, structure, concentration, and biochemical formation, the degradation mechanisms are still unresolved.

3.4 Acidification in the polar ocean

The rapid increase of the partial pressure of carbon dioxide (pCO_2) in the atmosphere has an impact on the carbonate system in the oceanic surface layer and, with delay, also in the deeper ocean. The uptake of CO_2 by the oceanic surface layer leads to a rearrangement in the carbonate system where carbonate ions are lost and protons (H^+) gained, i.e. the pH decreases. This process is commonly known as ocean acidification (OA; note that despite large changes the oceanic pH remains in the alkaline realm, i.e. pH >7). The substantial pH-changes that have occurred in the Anthropocene (Rhein et al. 2013) are caused by CO_2 emissions at a much larger rate than the ocean-wide overturning and response of carbonate-rich sediments (the latter of which would be able to counter pH changes). Another predominant effect of OA is the decrease in the saturation state of the two main forms of carbonate minerals, namely aragonite and calcite. It must be accounted for that pH and the carbonate ion concentration are subject to a seasonal cycle with high values in summer, due to drawdown of CO_2 by photosynthesis and low pH and carbonate in winter (Fig. 22b). Uncertainty in the seasonal signal is still prevailing, which is further demonstrated by Roden et al. (2013), who compared two annual cycles of pH at the same station in the Indian sector of the Southern Ocean and found a factor-of-two difference in amplitude.

Measurements of pH in the Southern Ocean for documenting the progress of OA are scarce, but fortunately, data from other variables of the carbonate system can be used to compute pH (and the carbonate ion concentration). Because pCO_2 and pH are linked via a strong anti-correlation, the surface ocean pCO_2 data of Takahashi et al. (2009) can be used to illustrate the large-scale OA. Full-blown acidification of the Southern Ocean is evidenced by these data showing that the ocean roughly follows the atmospheric CO_2 increase. On a smaller scale in the Weddell Gyre, a pH decrease of about 0.01 per decade (and a concomitant decrease of the carbonate ion concentration) was estimated from repeat section data of the carbonate system covering few decades (Fig. 24, Hauck et al. 2010; Van Heuven et al. 2011). The Weddell Gyre may be different from the remaining Southern Ocean as the changes would be somewhat less (Hauck et al. 2010). Also, in the bottom water of the Weddell Sea, which carries remnants of surface water, significant reductions—slightly less than in the surface layer—of pH were found (Van Heuven et al. 2011). Hauck et al. (2010) estimate that aragonite undersaturation in the Weddell Sea under steady conditions will not occur before 2100 (and for calcite even later than that). In contrast, McNeil and Matear (2008) suggest that undersaturation may become reality as early as the 2030s in a coastal region east of the Weddell Gyre.

It is obvious that OA is driven by the atmospheric burden of anthropogenic CO_2, which brings CO_2 into the surface

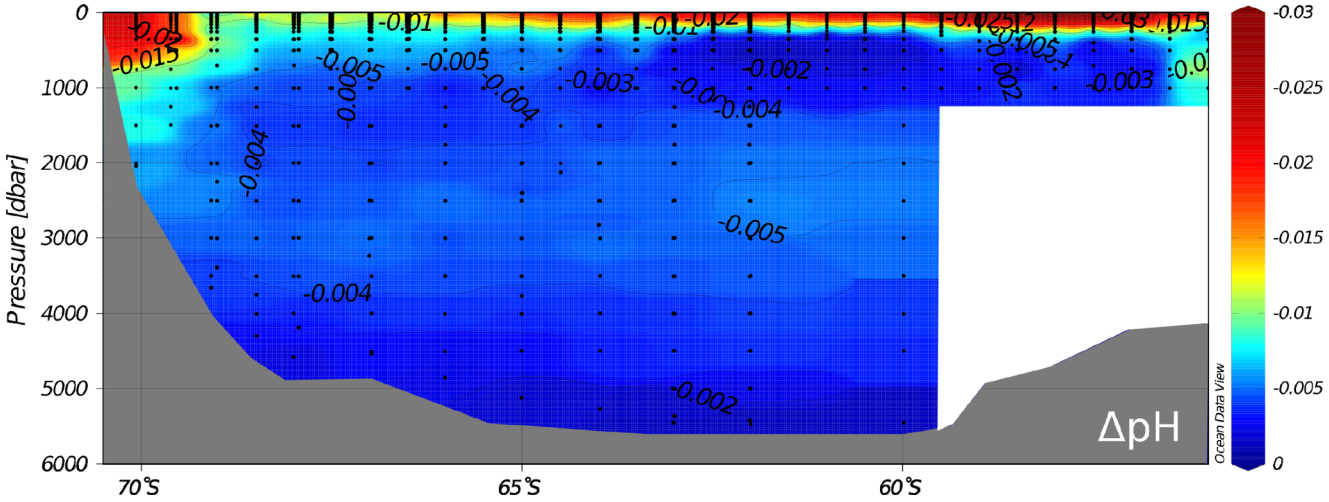

Fig. 24 Change in acidification (pH) between 1992 and 2008 in the Weddell Sea at the Prime Meridian (location see Fig. 18), modified from Hauck et al. (2010)

layer and changes the carbonate equilibrium, diminishing pH and the carbonate ion concentration. This mechanism will continue in the future, possibly at an even higher rate due to the expected faster rise in atmospheric CO_2. The future increase of the Revelle factor as a consequence of a higher CO_2 level of the surface water will slow down the CO_2 uptake and hence the acidification rate to some extent, although this might not be the case in the southern Weddell Sea where the CO_2 uptake rate might continue to grow with a higher Revelle factor (Hauck and Völker, 2015). At the same time, the rate of acidification per CO_2 uptake might increase as the carbonate equilibria shift to higher CO_2 concentrations. Altogether, these processes will likely lead to higher acidification rates in the future. Via the formation of ventilated deep and bottom waters, the acidification is passed on to the deeper realms of the Weddell Sea and from there to the global ocean; the typical time scale is hundreds to thousands of years. An ice cover tends to slow down OA because the sea ice prevents a full equilibration of ocean and atmosphere. A further effect of sea-ice formation in winter is a reduction of alkalinity of the underlying water, i.e. within the ice, calcium carbonate precipitates in the brine channels. This deteriorates the level of acidification seasonally. It is not clear where the balance of these counteracting processes by sea ice lies, but it is likely to be spatially variable. In addition, decreasing ventilation of the deep Weddell Sea (see Section 3.2) is already slowing down the uptake of anthropogenic CO_2 (Huhn et al. 2013) and, thus, the acidification. Even so, the shallow sediments of the Southern Ocean do not contain sufficient carbonate to buffer the enhanced acidification (Hauck et al. 2013a).

The consequences of ocean acidification are likely to be numerous, ranging from changes in chemical speciation of metals (Millero et al. 2009) to changes in absorption of sound waves (Ilyina et al. 2009), and major or minor impact on marine ecosystems (Wittmann and Portner, 2013) with consequences for the structure and functioning of ecosystems and biogeochemical cycles (Gattuso and Hansson 2011; Doney et al. 2012).

3.5 Trace elements and the nutrient cycle

In addition to the carbon sequestration mechanisms highlighted in Section 3.3, C_{ant} is transported from the surface layer into the ocean interior via the biological carbon pump: carbon is taken up by primary production and sinks down the water column as particulate organic matter and calcareous particles and ultimately gets stored in the ocean sediment. Microbial respiration, heterotrophic bacteria (Obernosterer et al. 2008; Jiao and Azam 2011) and photochemical degradation affect the efficacy of the biological pump and the conversion between dissolved and particulate carbon pools. The fluxes depend on the availability of macronutrients (nitrate, phosphate, ammonium and silicate); trace elements (such as iron, manganese, zinc, cadmium); oxygen; temperature; and light availability. Anthropogenic changes in CO_2 can also stimulate primary productivity and change the structure of phytoplankton assemblages, therewith affecting the potential for carbon export (Tortell et al. 2008; Hoppe et al. 2013; Trimborn et al. 2013). In the following, we review recent studies that give insight into primary productivity, micronutrient utilization (Fe, Zn Cd, Th, and Pa). The final paragraph infers oceanic mixing and continental weathering sources based on Nd and Hf isotopes.

Iron availability is considered the primary control for biological carbon fixation in the Southern Ocean, contributing about half of the annual carbon fixation from atmospheric CO_2. According to the iron hypothesis raised by Martin (1990), stimulation of the biological pump by increased atmospheric supply of iron-containing dust to the Southern Ocean during the drier cold climate periods explains the lowering of

CO_2 in the atmosphere during glacial periods, which is documented in ice cores. While many ocean iron fertilization experiments provided support for the first part of the iron hypothesis, the stimulation of phytoplankton primary production, a recent study also supported the second part, namely the carbon export from an iron-stimulated phytoplankton bloom to the deep ocean (Smetacek et al. 2012). However, extrapolating the results of such mesoscale experiments to larger space and time scales is hardly possible. In part, it is hampered by the complexity of interactions between the species, which builds the marine food web. Complexity begins already at the level of the primary producers, even within the genus of the diatoms, of which some act as carbon sinkers while others drain predominately silicate (Assmy et al. 2013). The species distribution in turn is influenced by the physical environment—the variables of ocean state, currents, and turbulence regime.

Zn is another essential trace metal for phytoplankton, and culture studies have suggested that its uptake may be influenced by the availability of Fe. Cd can also be taken up by phytoplankton and may substitute Zn in cambialistic carbonic anhydrases, which are involved in the uptake of inorganic carbon. Studying both elements in the Southern Ocean is also of interest because of their use as paleo-tracers for past ocean circulation and nutrient availability. Speciation measurements south of the Polar Front reveal high concentrations of dissolved bioavailable Zn (Baars and Croot, 2011) and Cd (Baars et al. 2014) that help to explain high apparent Zn/P and Cd/P uptake ratios in the Southern Ocean (Croot et al. 2011; Baars et al. 2014). Local changes in potential Cd uptake rates, inferred from Cd* (defined as the deviation of total dissolved Cd from a linear deep water Cd vs. P relation), suggest that the Cd/P uptake ratios are also dependent on the availability of Zn, Mn, and Fe, which leads to a peculiar band of negative Cd* in sub-Antarctic mode water and Antarctic Intermediate Water (Baars et al. 2014; Fig. 25).

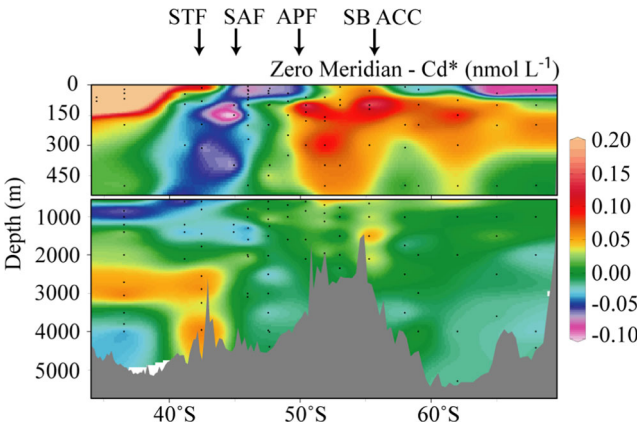

Fig. 25 Distribution of Cd*, defined as deviations of measured dissolved Cd from a linear Cd vs. P relation (Baars et al. 2014). *STF* Subtropical Front, *SAF* Subantarctic Front, *APF* Antarctic Polar Front, *SB ACC* Southern boundary of the Antarctic Circumpolar Current

The distribution of Cd isotopes (Abouchami et al. 2011; Xue et al. 2013; Abouchami et al. 2014) shows a contrast between deep and surface waters with biological uptake dictating the surface layer signature (Fig. 26b). The deep water signal is determined by the flux of regenerated isotopically light Cd from sinking organic matter and the degree of mixing of distinct water masses (Fig. 26). A correlation between Cd and Zn isotopes (Zhao et al. 2014) in different nutrient and ecological regimes of the Southern Ocean points to a strong link between Cd stable isotope fractionation and Zn availability. The suggested dependence of Cd/P and Zn/P uptake on the availability of other trace metals, most importantly Fe, has clear implications for their use as paleo-tracers of past deep water circulation and nutrient utilization. Further culture studies are needed to fully understand the physiological mechanisms governing the uptake and resulting isotope fractionation of Cd and Zn in the oceans and will be paramount for establishing a link with the global carbon cycle.

^{230}Th and ^{231}Pa have been used to estimate the export flux of particulate organic carbon as well as trace-metal scavenging processes. ^{230}Th and ^{231}Pa data (Venchiarutti et al. 2011) indicate that distributions in the Atlantic sector of the Southern Ocean are mainly driven by reversible-scavenging mechanisms and the southward upwelling of radionuclide-rich deep water masses. High resolution mapping of particulate and dissolved ^{234}Th in surface water in comparison with satellite chlorophyll-a and trace metal data showed the time lag of 1–2 months between bloom development and the export of adsorbed trace elements to depth (Rutgers van der Loeff et al. 2011). However, bottom scavenging or scavenging in opal rich areas locally create significant variations in these radionuclide distributions. Near the Antarctic Peninsula, thorium isotopes (^{234}Th and ^{232}Th) combined with trace metals (Al, Mn, Fe; Middag et al. (2011a, b); Klunder et al. (2011)) showed signatures highly influenced by terrigenous inputs and effects of sediment resuspension. Settling diatoms in the ACC form an efficient sink for ^{231}Pa that accumulates at mid-depth, while bottom waters are again depleted in ^{231}Pa by contact with opal-rich sediments.

Dissolved hafnium (Hf) and neodymium (Nd) in seawater are of lithogenic origin and are introduced via weathering inputs, dissolution of particles, or seawater-sediment interactions. Their respective radiogenic isotope compositions (^{143}Nd/^{144}Nd expressed as εNd and ^{176}Hf/^{177}Hf expressed as εHf in parts per 10,000) in sea water allow the evaluation of the continental source rocks and weathering regimes (e.g. Piepgras and Wasserburg 1982; van de Flierdt et al. 2002; Bayon et al. 2006). In the first detailed study of the Hf and Nd distributions in the Atlantic sector of the Southern Ocean, only one surface sample had a significantly higher εHf (+6.1) and εNd (−4.0) as a consequence of local weathering inputs from the volcanic King George Island (Stichel et al. 2012b). Markedly negative εNd values coinciding with high Nd

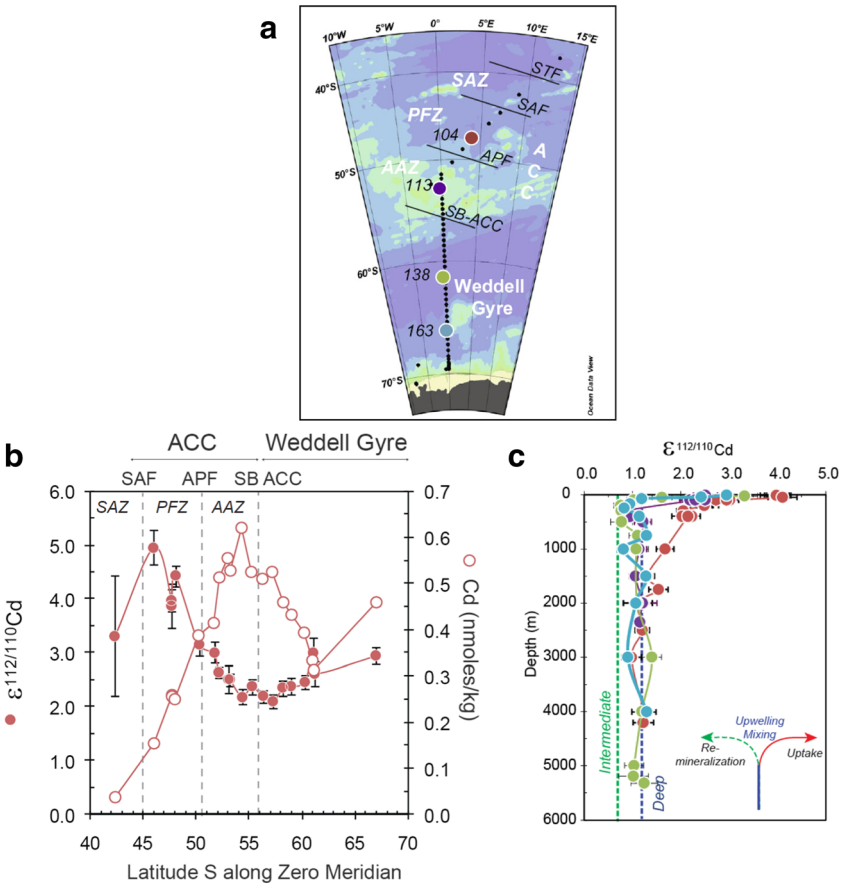

Fig. 26 **a** Location map of samples and stations collected for Cd isotope analyses during cruise Ant XXIV/3 along the Prime Meridian. *STF* Subtropical Front, *SAF* Subantarctic Front, *SAZ* Subantarctic Zone, *PFZ* Polar Frontal Zone, *AAZ* Antarctic Zone, *APF* Antarctic Polar Front, *ACC* Antarctic Circumpolar Current, *SB-ACC* Southern boundary of the Antarctic Circumpolar Current. **b** Latitudinal variations in Cd concentrations and Cd isotope ratios expressed as $^{112/110}$Cd (defined as $[(^{110}Cd/^{112}Cd)_{NIST}/(^{110}Cd/^{112}Cd)_{Sa} - 1] \times 10^4$) (Abouchami et al. 2012). **c** Vertical distribution of $^{112/110}$Cd at the four stations shown (**a**). The *arrows* illustrate the effect of biological uptake and remineralization on the Cd isotopic composition of the water. Surface waters are 'heavy' due to preferential uptake by phytoplankton of the 'light' Cd isotope, while 'light' Cd in deeper waters is acquired from recycled organic matter

concentrations and continental rock-like rare earth elements pattern in surface waters were found 200 km off South Africa, indicating weathering inputs from old continental crust (Stichel et al. 2012b).

Hf consistently shows the lowest concentrations in the surface waters within the Polar Frontal Zone and systematically increases south of the ACC (Stichel et al. 2012b). The concentrations of both elements increase with water depth. Within the ACC, the increase in Nd is nearly linear and correlates well with dissolved Si, indicative of a vertical flux controlled by desorption of scavenged Nd from diatom frustules (Stichel et al. 2012a). The Hf concentration shows a less pronounced increase with depth and remains essentially constant below 1500 m suggesting shallower remineralisation. Within the Weddell Gyre Nd concentrations follow a pattern similar to Hf with increasing values only in the uppermost 1 km of the water column (Stichel et al. 2012a). The limited increase coincides with low particle fluxes and a shallow remineralisation depth documented by the vertical distribution of excess ^{234}Th, which has been detectable in the upper few hundred meters in the Weddell Gyre (Usbeck et al. 2002). Additionally, the high concentrations in the Weddell Gyre are promoted by upwelling of the densest modes of CDW (Stichel et al. 2012a,b).

The Nd isotope composition in CDW can be almost solely explained by mixing of deep water masses coming from the North Atlantic and North Pacific (Stichel et al. 2012b), while Nd concentrations in CDW are governed by a non-conservative behaviour (Stichel et al. 2012a). Antarctic Bottom Water concentrations at the Prime Meridian indicate interactions with the continental shelf off East Antarctica. The observed isotope signature suggests a source region of AABW at about 60° E, east of the Weddell Gyre (Meijers et al. 2010; Stichel et al. 2012a).

4 Summary and conclusions

4.1 Atmosphere

The main challenges that were addressed by the DFG Antarctic program funded research were to improve the simulation of Antarctic climate and understanding the interaction between atmosphere, ice and ocean. The related research showed significant progress towards more realistic simulations and towards a deeper understanding and improved quantification of the involved processes.

Germany contributed to the long-term monitoring of the ozone layer by continuous measurements starting in 1985. It was found that Antarctic springtime ozone depletion shows large interannual variations and is strongly correlated with a

cooling of the stratosphere. So far, the observations are inconclusive regarding a recent recovery of the Antarctic ozone.

The simulation of ozone-related changes in atmospheric circulation and sea ice extent using the EMAC chemistry-climate model reveals a positive correlation between the Southern Annular Mode index and sea ice extent on interannual time scales in agreement with observations. Due to these results, for the second half of the twenty-first century, when total column ozone is projected to recover, the GHG induced climate change will dominate and Antarctic sea ice concentration will decrease. Multi-model ensemble coupled atmosphere-ocean general circulation model simulations show that climate change impacts on extra-tropical cyclones (ETCs) lead to a decrease of the total number of cyclones at the end of the twenty-first century, but the number of extremely strong ETCs increases.

The regional climate model simulations (HIRHAM4) with a horizontal resolution of 50 km made significant progress with regard to the water cycle over Antarctica. Covering the years 1958 to 1998, the mean atmospheric circulation, synoptic weather systems, and the spatial distribution of precipitation minus sublimation structures are realistically simulated. The observed increase in surface mass accumulation at the West Antarctic coasts and reductions in parts of East Antarctica could be explained by the modelled P-E trends.

The parameterization of sub grid-scale processes is still a great challenge for climate research. Work funded by the DFG concentrated on the parameterization of turbulence with a focus on convection studies over leads and during cold-air outbreaks. Using the Large Eddy Simulation model PALM, cases with and without organized roll convection were investigated with the focus on vertical turbulent fluxes. A striking finding was that these fluxes do not differ between roll and non-roll cases. This implies that a development of additional parameterization schemes accounting for specific characteristics of roll convection is not necessary in numerical weather prediction and climate models. On the other hand, the impact of leads on the surface energy balance has been found to be substantial. Progress has been obtained with the parameterizations of the lead-generated turbulence in microscale models. The necessary studies helped to better understand the complex processes over leads. However, parameterizations of the lead impact on energy and momentum fluxes and their non-linear dependence on the sea ice concentration need still improvements in forthcoming climate models. In this respect, the strategy of involving LES and micro/mesoscale modelling in the parameterization development has proven to be promising.

In the marginal seas of the Southern Ocean, katabatic winds and polynyas are features important for the air-sea fluxes. At Luitpold Coast, the link between katabatic winds and polynya formation was studied with the high-resolution (5 km) non-hydrostatic atmospheric model COSMO for the winter season. Changes in polynya area are mainly controlled by the downslope component of the surface wind, which offshore component is mainly steered by a pressure gradient due to katabatic force. The study was supplemented with regard to polynya and dense shelf water formation using the finite element sea ice ocean model FESOM for the southern Weddell Sea. A large sensitivity of coastal polynya formation to the atmospheric forcing is found. Major differences occur in mountainous areas where the wind is strongly influenced by surface topography. Thus, high-resolution atmospheric models are needed to provide realistic forcing for sea ice-ocean models in the Weddell Sea area. The model efforts were complemented by a long-term study for coastal polynyas using MODIS thermal-infrared imagery. Thin-ice thickness and sea-ice production were determined on a daily basis with a high spatial resolution of 2 km. The most efficient sea ice production areas are the polynyas off Ronne and Brunt Ice Shelves. All regions show a high interannual variability and, except for Coats Land, a negative trend for sea ice production. The high-resolution (2 km) data set represents a new benchmark for the validation of model estimates of sea ice production in Weddell Sea polynyas.

4.2 Ocean

Combining observations and state-of-the-art numerical models, the German efforts in the ocean focused on the changes in circulation and water mass ventilation, and the impact of these changes on ice shelf melting as well as the distribution of trace elements and climate relevant trace gases such as CO_2.

Starting in 1984, the monitoring at a high-resolution hydrographic section along the Prime Meridian represents the longest time series in the Southern Ocean. Together with a section across the central Weddell Sea, it constitutes the major portion of hydrographic data from the Atlantic sector of the Southern Ocean. The AABW formation rate inferred from the current meter observations (3–4 Sv) corresponds to inverse modelling approaches (5–6 Sv) and other hydrography or tracer-based estimates (4–5 Sv). Recently, indications for changing water mass properties and a possible reduction of deep and bottom ventilation in the Weddell Sea have emerged. The CTD sections (1984 to 2008) reveal a significant warming in the deep waters, while WSDW became saltier and WSBW fresher. Moreover, the cross section area occupied by WSBW at the Prime Meridian declined by 25 %. Based on long-term CFC time series, all deep water masses within the Weddell Sea have been continually getting older and less ventilated during the last 27 years. The decline of the ventilation rate of WSDW and WSBW by 18–23 % seems to be mainly caused by mixing with WDW, which aged much faster by 35 %.

Despite their relevance, the variability of ventilation and formation rates of deep and bottom waters and the related storage of C_{ant} in the Southern Ocean is currently not well constrained. Numerical models with very high resolution are

promising and necessary to account for the complex atmosphere-ocean-sea ice-interaction and for irregularities in the bottom topography. In union with the reduced ventilation of the deep and bottom waters, C_{ant} uptake and storage slowed down by 14–21 % as compared to the steady state situation with level ventilation. The mechanism behind the reduction of C_{ant} uptake in the Weddell Sea may well be an elevated upwelling of subsurface water, which occurred at least during the 1990s and 2000s. Downwelling of dissolved organic carbon (DOC) in the Weddell Sea contributes to the buffer in the ocean carbon cycle. It is not clear how this carbon buffer will evolve in the future global biogeochemical cycle and how it affects the climate system. Further removal of DOC depends primarily on microbial degradation and light availability (photo degradation). Via the formation of ventilated deep and bottom waters, the acidification is passed on to the deeper realms of the Weddell Sea and from there to the global ocean with a typical time scale of hundreds to thousands of years. In the bottom water of the Weddell Sea significant reductions—slightly less than in the surface layer—of pH were found. However, the onset of an aragonite undersaturation in the Weddell Sea is still under debate—under steady conditions it might not occur before year 2100 (for calcite even later) or as early as the 2030s in a coastal region east of the Weddell Gyre.

Using He and Ne isotope observations, including the hydrographic data along the aforementioned sections, the contribution of glacial melt to the Weddell Sea water masses is estimated to be 35 ± 19 Gt year^{-1} (1 Gt = 10^9 tons) for the Larsen (LIS) and 123 ± 53 Gt year^{-1} for the Filchner-Ronne Ice Shelves (FRIS). These numbers are a mean over several decades. Melt water more directly fed into the world ocean originates from the LIS fringing the western Weddell Sea. Part of this freshwater remains on the northwestern Weddell Sea continental shelf causing a freshening of the winter shelf water column and a salinity decrease of the deep waters in the central basin of Bransfield Strait. Projections, based on IPCC AR4 climate scenarios, show that the density structure on the southern Weddell Sea continental shelf may allow the slope current to penetrate into the Filchner Trough transporting warm water of open ocean origin to the deep FRIS grounding line. This might boost the basal mass loss by roughly a factor of 10. The associated thickness decrease has severe consequences for the buttressing potential of the ice shelf and the dynamics of the ice streams draining East Antarctica. The increase in glacial meltwater also freshens the western Weddell Sea continental shelf, reducing the basal melting of LIS. This indicates a link between the different ice shelves via the continental shelf and slope circulations and calls for circumpolar rather than regional approaches if the interaction of the Southern Ocean with Antarctic ice shelves is investigated.

Many ocean iron fertilization experiments provided support for the stimulation of phytoplankton primary production, but a recent study also supports the carbon export from an iron-stimulated phytoplankton bloom to the deep ocean. Extrapolating the results of such mesoscale experiments to larger space and time scales is hardly possible, in part, due to the complexity of interactions between the species building the marine food web. Complexity begins already at the level of the primary producers, even within the genus of the diatoms of which some act as carbon sinkers while others drain predominately silicate. The dependence of Cd/P and Zn/P uptake on the availability of other trace metals, most importantly Fe, has clear implications for their use as paleo-tracers of past deep water circulation and nutrient utilization. Culture studies are needed to fully understand the physiological mechanisms governing the uptake and resulting isotope fractionation of Cd and Zn in the oceans, and they will be paramount for establishing a link with the global carbon cycle.

High-resolution mapping of particulate and dissolved ^{234}Th in surface water in comparison with satellite chlorophyll-a and trace metal data shows a time lag of 1–2 months between bloom development and the export of absorbed trace elements to depth. However, bottom scavenging or scavenging in opal-rich areas create locally significant variations in these radionuclide distributions. Near the Antarctic Peninsula, thorium isotopes (^{234}Th and ^{232}Th) combined with trace metals (Al, Mn, Fe) show signatures highly influenced by terrigenous inputs and effects of sediment resuspension while Antarctic Bottom Water concentrations at the Prime Meridian indicate interactions with the continental shelf off East Antarctica. The observed isotope signature suggests a source region of AABW at about 60° E, east of the Weddell Gyre.

In summary, German Antarctic research of the last decade in collaboration with international partners fostered significantly our understanding of a variety of climate relevant processes in the atmosphere and the ocean as well as at their interface.

Acknowledgments Much of the research presented here would have not been possible without the funding through the DFG SPP-1158 'Antarctic Research'. We also thank the captains and crews of the icebreaker POLARSTERN, the aircraft crews, the personnel of the Antarctic stations, and the logistic department of the Alfred Wegener Institute.

References

Abouchami W, Galer SJG, De Baar HJW, Alderkamp AC, Middag R, Laan P, Feldmann H, Andreae MO (2011) Modulation of the Southern Ocean cadmium isotope signature by ocean circulation and primary productivity. Earth Planet Sci Lett 305:83–91

Abouchami W, Galer SJG, Horner TJ, Rehkämper M, Wombacher F, Xue Z, Lambelet M, Gault-Ringold M, Stirling CH, Schönbächler M,

Shiel AE, Weis D, Holdship PF (2012) A common reference material for cadmium isotope studies—NIST SRM 3108. Geost Geoanal Res. doi:10.1111/j.1751-908X.2012.00175

Abouchami W, Galer SJG, De Baar HJW, Middag R, Vance D, Zhao Y, Klunder M, Mezger K, Feldmann H, Andreae MO (2014) Biogeochemical cycling of cadmium isotopes in the Southern Ocean along the zero meridian. Geochim Cosmochim Acta 127: 348–367

Adams S, Willmes S, Schröder D, Heinemann G, Bauer M, Krumpen T (2013) Improvement and sensitivity analysis of thermal-thin-ice retrievals. IEEE Trans Geosci Remote Sens 51:3306–3318. doi:10.1109/TGRS.2012.2219539

Anderson LG, Holby O, Lindegren R, Ohlson M (1991) The transport of anthropogenic carbon dioxide into the Weddell Sea. J Geophys Res 96:16679–16687

Andreas EL, Cash BA (1999) Convective heat transfer over wintertime leads and polynyas. J Geophys Res 104:25,721–25,734

Arndt JE (2013) The International Bathymetric Chart of the Southern Ocean (IBCSO) – Digital Bathymetric Model. Alfred Wegener Institute Helmholtz Centre for Polar and Marine Research, Bremerhaven. doi:10.1594/PANGAEA.805734

Assmy P, Smetacek V, Montresor M, Klaas C, Henjes J, Strass V, Arrieta JM, Bathmann UV, Berg GM, Breitbarth E, Cisewski B, Friedrichs L, Fuchs N, Herndl GJ, Jansen S, Krägefsky S, Latasa M, Peeken I, Röttgers R, Scharek R, Schüller SE, Steigenberger S, Webb A, Wolf-Gladrow D (2013) Thick-shelled, grazer-protected diatoms decouple ocean carbon and silicon cycles in the iron-limited Antarctic circumpolar current. Proc Natl Acad Sci U S A. doi:10.1073/pnas.1309345110

Baars O, Croot PL (2011) The speciation of dissolved zinc in the Atlantic sector of the Southern Ocean. Deep-Sea Res II 58(25–26):2720–2732

Baars O, Abouchami W, Galer SJG, Boye M, Croot PL (2014) Dissolved cadmium in the Southern Ocean: distribution, speciation, and relation to phosphate. Limnol Oceanogr 59:385–399

Bayon G, Vigier N, Burton KW, Jean Carignan AB, Etoubleau J, Chu N-C (2006) The control of weathering processes on riverine and seawater hafnium isotope ratios. Geology 34(433). doi:10.1130/G22130.1

Broecker WS, Peacock SL, Wallace S (1997) How much deep water is formed in the Southern Ocean? J Geophys Res 103:15833–15843

Broecker WS, Suttherland S, Peng TH (1999) A possible 20th-century slowdown of Southern Ocean deep water formation. Science 286: 1132–1135

Bromwich DH, Monaghan AJ, Manning KW, Powers JG (2005) Real-time forecasting for the Antarctic: an evaluation of the Antarctic mesoscale prediction system (AMPS). Month Weath Rev 133: 581–603

Bromwich DH, Nicolas JP, Monaghan AJ (2011) An assessment of precipitation changes over Antarctica and the Southern Ocean since 1989 in contemporary reanalyses. J Clim 24:4189–4209

Brümmer B (1999) Roll and cell convection in wintertime Arctic cold-air outbreaks. J Atmos Sci 56:2613–2636

Brümmer B, Pohlmann S (2000) Wintertime roll and cell convection over Greenland and Barents Sea regions: a climatology. J Geophys Res 105:15,559–15,566

Bullister J, Rhein M, Mauritzen C (2013) Deep water formation. In: Siedler G, Church J, Gould J, Griffies S (eds) Ocean circulation and climate—observing and modelling the global ocean, 2nd edn. Academic Press, Oxford ISBN 978-0-12-391851-2

Carlson CA, Hansell DA, Nelson NB, Siegel DA, Smethie WM, Khatiwala S, Meyers MM, Halewood E (2010) Dissolved organic export and subsequent remineralization in the mesopelagic and bathypelagic realms of the North Atlantic Ocean. Deep-Sea Res I 57:1433–1445

Chechin DG, Lüpkes C, Repina IA, Gryanik VM (2013) Idealized dry quasi 2-D mesoscale simulations of cold-air outbreaks over the marginal sea ice zone with fine and coarse resolution. J Geophys Res 118:8787–8813. doi:10.1002/jgrd.50679

Cisewski B, Strass V, Leach H (2011) Circulation and transport of water masses in the Lazarev Sea, Antarctica, during summer and winter 2006. Deep Sea Res I 58:186–199. doi:10.1016/j.dsr.2010.12.001

Comiso JC, Parkinson CL, Gersten R, Stock L (2008) Accelerated decline in the Arctic sea ice cover. Geophys Res Lett 35(L01703). doi:10.1029/2007GL031972

Cordero RR, Damiani A, Seckmeyer G, Riechelmann S, Laroze D, Garate F, Labbe F (2013) Satellite-derived UV climatology at Escudero Station (Antarctic peninsula). Ant Sci 25(6):791–803. doi:10.1017/S0954102013000175

Cordero RR, Seckmeyer G, Damiani A, Riechelmann S, Rayas J, Labbe F, Laroze D (2014) Southern hemisphere's highest levels of surface UV: a case study. Photochem Photobiol Sci 13(1):70–81. doi:10.1039/C3PP50221J

Croot PL, Baars O, Streu P (2011) The distribution of dissolved zinc in the Atlantic sector of the Southern Ocean. Deep-Sea Res II 58(25–26):2707–2719

Crutzen PJ, Arnold F (1986) Nitric acid cloud formation in the cold Antarctic stratosphere: a major cause for the springtime "ozone hole. Nature 324:651–655

Denman KL, Brasseur G, Chidthaisong A, Ciais P, Cox PM, Dickinson RE, Hauglustaine D, Heinze C, Holland E, Jacob D, Lohmann U, Ramachandran S, Da Silva Dias PL, Wofsy SC, Zhang X (2007) Couplings between changes in the climate system and biogeochemistry. In: Solomon S, Qin D, Manning M, Chen Z, Marquis M, Averyt KB, Tignor M, Miller HL (eds) Climate change 2007: the physical science basis. Contribution of working group I to the fourth assessment report of the intergovernmental panel on climate change. Cambridge University Press, Cambridge

Depoorter MA, Bamber JL, Griggs JA, Lenaerts JTM, Ligtenberg SRM, van den Broeke M, Moholdt G (2013) Calving fluxes and basal melt rates of Antarctic ice shelves. Nature 502:89–92. doi:10.1038/nature12567

Dethloff K, Glushak K, Rinke A, Handorf D (2010) Antarctic 20th century accumulation changes based on regional climate model simulations. Adv Meteorol ID 327172 14 pp. doi: 10.1155/2010/327172.

Doney SC, Ruckelshaus M, Duffy JE, Barry JP, Chan F, English CA, Galindo HM, Grebmeier JM, Hollowed AB, Knowlton N, Polovina J, Rabalais NN, Sydeman WJ, Talley LD (2012) Climate change impacts on marine ecosystems. Ann Rev Mar Sci 4:11–37

Dotto TS, Kerr R, Mata MM, Azaneu M, Wainer I, Fahrbach E, Rohardt G (2014) Assessment of the structure and variability of Weddell Sea water masses in distinct ocean reanalysis products. Ocean Sci 10: 523–546. doi:10.5194/os-10-523-2014

Drucker R, Martin S, Kwok R (2011) Sea ice production and export from coastal polynyas in the Weddell and Ross seas. Geophys Res Lett 38(L17502). doi:10.1029/2011GL048668

Druffel ERM, Bauer JE (2000) Radiocarbon distributions in Southern Ocean dissolved and particulate organic matter. Geophys Res Lett 27:1495–1498

Dutrieux P, De Rydt J, Jenkins A, Holland PR, Ha HK, Lee SH, Steig EJ, Ding Q, Abrahamsen EP, Schröder M (2014) Strong sensitivity of Pine Island ice-shelf melting to climate variability. Science 343: 174–178. doi:10.1126/science.1244341

Ebner L, Heinemann G, Haid V, Timmermann R (2014) Katabatic winds and polynya dynamics at Coats Land, Antarctica. Ant Sci 26:309–326. doi:10.1017/S0954102013000679

Eden C, Jung T (2001) North Atlantic Interdecadal variability: oceanic response to the North Atlantic oscillation (1865–1997. J Clim 14: 676–691. doi:10.1175/1520-0442(2001)014<0676:NAIVOR>2.0.CO;2

Esau IN (2007) Amplification of turbulent exchange over wide arctic leads: Large-eddy simulation study. J Geophys Res 112(D08109). doi:10.1029/2006JD007225

Fahrbach E, Knoche M, Rohardt G (1991) An estimate of water mass transformation in the southern Weddell Sea. Mar Chem 35:25–44. doi:10.1016/S0304-4203(09)90006-8

Fahrbach E, Hoppema M, Rohardt G, Schröder M, Wisotzki A (2004) Decadal-scale variations of water mass properties in the deep Weddell Sea. Ocean Dyn 54:77–91. doi:10.1007/s10236-003-0082-3

Fahrbach E, Hoppema M, Rohardt G, Boebel O, Klatt O, Wisotzki A (2011) Warming of deep and abyssal water masses along the Greenwich meridian on decadal time scales: the Weddell gyre as a heat buffer. Deep-Sea Res II 58:2509–2523. doi:10.1016/j.dsr2,2011.06.007

Foldvik A, Gammelsrød T, Tørresen T (1985) Circulation and water masses on the southern Weddell Sea shelf. In: Jacobs SS (ed) Oceanology of the Antarctic continental shelf, Ant Res Seri 43:5–20 AGU Washington

Foldvik A, Gammelsrød T, Østerhus S, Fahrbach E, Rohardt G, Schröder M, Nicholls KW, Padman L, Woodgate RA (2004) Ice Shelf Water overflow and bottom water formation in the southern Weddell Sea. J Geophys Res 109(C02015). doi: 10.1029/2003JC002008

Foster TD, Carmack EC (1976) Frontal zone mixing and Antarctic bottom water formation in the southern Weddell Sea. Deep-Sea Res 23: 301–317

Garcia CAE, Mata MM (2005) Deep and bottom water variability in the central basin of Bransfield Strait (Antarctica) over the 1980–2005 period. CLIVAR Exchanges 10:48–50

Gattuso JP, Hansson L (eds) (2011) Ocean acidification. Oxford University Press

Gillett N, Thompson DW (2003) Simulation of recent southern hemisphere climate change. Science 302:273–275

Gordon AL (1998) Western Weddell Sea thermohaline stratification. In: Jacobs SS, Weiss RF (eds) Ocean, ice and atmosphere: interactions at Antarctic continental margins. Ant Res Seri 75:215–240 AGU Washington

Gordon AL, Huber B, Hellmer HH, Ffield A (1993) Deep and bottom water of the Weddell Sea's western rim. Science 262:95–97. doi:10.1126/science.262.5130.95

Gordon AL, Visbeck M, Huber B (2001) Export of Weddell Sea deep and bottom water. J Geophys Res 106:9005–9017

Grieger J, Leckebusch GC, Donat MG, Schuster M, Ulbrich U (2014) Southern hemisphere winter cyclone activity under recent and future climate conditions in multi-model AOGCM simulations. Int J Climatology 34:3400–3416. doi:10.1002/joc.3917

Grieger J, Leckebusch GC, Ulbrich U (2015) Net precipitation of Antarctica: thermodynamical and dynamical parts of the climate change signal. J Clim. doi:10.1175/JCLI-D-1400787.1 in press

Gryschka M, Drüe C, Etling D, Raasch S (2008) On the influence of sea-ice inhomogeneities onto roll convection in cold-air outbreaks. Geophys Res Lett 35(L23804). doi:10.1029/2008GL035845

Gryschka M, Fricke J, Raasch S (2014) On the impact of forced roll convection on vertical turbulent transport in cold air outbreaks. J Geophys Res 119:12,513–12,532. doi:10.1002/2014JD022160

Haid V, Timmermann R (2013) Simulated heat flux and sea ice production at coastal polynyas in the southwestern Weddell Sea. J Geophys Res 118:2640–2652. doi:10.1002/jgrc.20133

Haid V, Timmermann R, Ebner L, Heinemann G (2015) Atmospheric forcing of coastal polynyas in the southwestern Weddell Sea. Ant Sci 27:388–402. doi:10.1017/S0954102014000893

Hansell D (2013) Recalcitrant dissolved organic carbon fractions. Annuv rev. Mar Sci 5:421–425

Hansell D, Carlson CA, Repeta J, Schlitzer R (2009) Dissolved organic matter in the ocean. Oceanography 22:202–2011

Hartmann J, Kottmeier C, Raasch S (1997) Roll vortices and boundary-layer development during a cold air outbreak. Bound-Layer Meteorol 84:45–65. doi:10.1023/A:1000392931768

Hauck, J (2013) Processes in the Southern Ocean carbon cycle: Dissolution of carbonate sediments and inter-annual variability of carbon fluxes. Rep Pol Mar Res 669. 122 pp AWI Bremerhaven Germany

Hauck J, Völker C (2015) Rising atmospheric CO_2 leads to large impact of biology on Southern Ocean CO_2 uptake via changes of the Revelle factor. Geophys Res Lett 42:1459–1464. doi:10.1002/2015GL063070

Hauck J, Hoppema M, Bellerby RGJ, Völker C, Wolf-Gladrow D (2010) Data-based estimation of anthropogenic carbon and acidification in the Weddell Sea on a decadal timescale. J Geophys Res 115(C03004). doi:10.1029/2009jc005479

Hauck J, Arrigo KR, Hoppema M, Van Dijken GL, Völker C, Wolf-Gladrow D (2013a) Insignificant buffering capacity of Antarctic shelf carbonates. Global Biogeoch Cycl 27:11–20. doi:10.1029/2011GB004211

Hauck J, Völker C, Wang T, Hoppema M, Losch M, Wolf-Gladrow D (2013b) Seasonally different carbon flux changes in the Southern Ocean in response to the southern annular mode. Global Biogeochem Cycl 27:1236–1245. doi:10.1002/2013GB004600

Heinemann G (1997) Idealized simulations of the Antarctic katabatic wind system with a three-dimensional meso-scale model. J Geophys Res 102:13825–13834

Hellmer HH (2004) Impact of Antarctic ice shelf melting on sea ice and deep ocean properties. Geophys Res Lett 31(L10307). doi:10.1029/2004GL19506

Hellmer HH, Huhn O, Gomis D, Timmermann R (2011) On the freshening of the northwestern Weddell Sea continental shelf. Ocean Sci 7: 305–316. doi:10.5194/os-7-305-2011

Hellmer HH, Kauker F, Timmermann R, Determann J, Rae J (2012) Twenty-first-century warming of a large Antarctic ice-shelf cavity by a redirected coastal current. Nature 485:225–228. doi:10.1038/nature11064

Hoppe CJM, Hassler CS, Payne CD, Tortell PD, Rost B, Trimborn S (2013) Iron limitation modulates ocean acidification effects in Southern Ocean phytoplankton communities. PLoS One 8(11): e79890. doi:10.1371/journal.pone.0079890

Hoppel K, Nedoluha G, Fromm M, Allen D, Bevilacqua R, Alfred J, Johnson B, König-Langlo G (2005) Changes in ozone loss at the upper edge of the Antarctic ozone hole during 1994–2005. Proc AGU Fall Meeting 2005 San Francisco

Hoppema M, Klatt O, Roether W, Fahrbach E, Bulsiewicz K, Rodehacke C, Rohardt G (2001) Prominent renewal of Weddell Sea deep water from a remote source. J Mar Res 59:257–279

Hoppema M, Bakker K, Van Heuven SMAC, Van Ooijen JC, De Baar HJW (2015) Long-term accurate nutrients along a repeat section through the Weddell Sea: distributions, trends and inter-annual variability (1996-2011. Mar Chem 177:545–553. doi:10.1016/j.marchem.2015.08.007

Huhn O, Hellmer HH, Rhein M, Roether W, Rodehacke C, Schodlok M, Schröder M (2008) Evidence of deep and bottom water formation in the western Weddell Sea. Deep-Sea Res II 55:1098–1116. doi:10.1016/j.dsr2.2007.12.015

Huhn O, Rhein M, Hoppema M, Van Heuven S (2013) Decline of deep and bottom water ventilation and slowing down of anthropogenic carbon storage in the Weddell Sea, 1984–2011. Deep-Sea Res Part I 76:66–84. doi:10.1016/j.dsr.2013.01.005

Ilyina T, Zeebe RE, Brewer PG (2009) Future ocean increasingly transparent to low-frequency sound owing to carbon dioxide emissions. Nature Geosci 3:18–22

IPCC 2013 Climate change 2013: the physical science basis. Contribution of Working Group I to the Fifth Assessment Report of the Intergovernmental Panel on Climate Change. In: Stocker TF,

Qin D, Plattner G-K, Tignor M, Allen SK, Boschung J, Nauels A, Xia Y, Bex V, Midgley PM (eds) Cambridge University Press, Cambridge. 1535 pp. doi:10.1017/CBO9781107415324

Jacobs SS, Hellmer HH, Doake CSM, Jenkins A, Frolich RM (1992) Melting of ice shelves and the mass balance of Antarctica. J Glaciol 38:375–387

Jacobs SS, Giulivi CF, Mele PA (2002) Freshening of the Ross Sea during the late twentieth century. Science 297:386–389

Jiao N, Azam, F (2011) Microbial carbon pump and its significance for carbon sequestration in the Ocean. Science Suppl 43–45

Jöckel P, Tost H, Pozzer A, Brühl C, Buchholz J, Ganzeveld L, Hoor P, Kerkweg A, Lawrence MG, Sander R, Steil B, Stiller G, Tanarhte M, Taraborelli D, Van Aardenne J, Lelieveld J (2006) The atmospheric chemistry general circulation model ECHAM5/MESSy: consistent simulation of ozone from the surface to the mesosphere. Atmos Chem Phys 6:5067–5104

Jonassen, M. O., Tisler, P., Altstädter, B., Scholtz, A., Vihma, T., Lampert, A., König-Langlo, G. and Lüpkes, C. (2015) Application of remotely piloted aircraft systems in observing the atmospheric boundary layer over Antarctic sea ice in winter. Polar Res 34(25651). doi:10.3402/polar.v34.25651

Jungclaus JH, Keenlyside N, Botzet M, Haak H, Luo JJ, Latif M, Marotzke J, Mikolajewicz U, Roeckner E (2006) Ocean circulation and tropical variability in the coupled model ECHAM5/MPI-OM. J Clim 19:3952–3972

Kern S (2009) Wintertime Antarctic coastal polynya area: 1992–2008. Geophys Res Lett 36(L14501). doi:10.1029/2009GL038062

Khatiwala S, Primeau F, Hall T (2009) Reconstruction of the history of anthropogenic CO_2 concentrations in the ocean. Nature 462:346–349. doi:10.1038/nature08526

King JC, Turner J (1997) Antarctic meteorology and climatology. Cambridge Univ. Press 409 pp

Klatt O, Roether W, Hoppema M, Bulsiewicz K, Fleischmann U, Rodehacke C, Fahrbach E, Weiss RF, Bullister JL (2002) Repeated CFC sections at the Greenwich meridian in the Weddell Sea. J Geophys Res 107. doi:10.1029/2000JC000731

Klunder MB, Laan P, Middag R, De Baar HJW, Van Ooijen JC (2011) Dissolved iron in the Southern Ocean (Atlantic sector). Deep-Sea Res II 58:2678–2694

Koch BP, Kattner G, Witt M, Passow U (2014) Molecular insights into the microbial formation of marine dissolved organic matter: recalcitrant or labile? Biogeosciences 11:4173–4190

König-Langlo G, Gernandt H (2009) Compilation of ozonesonde profiles from the Antarctic Georg-Forster-Station from 1985 to 1992. Earth Sys Sci Data 1:1–5. doi:10.5194/essd-1-1-2009

König-Langlo G, Loose B (2007) The meteorological observatory at Neumayer Stations (GvN and NM-II) Antarctica. Polarforschung 76:25–38

Kristovich DAR, Laird NF, Hjelmfelt MR, Derickson RG, Cooper KA (1999) Transitions in boundary layer meso-convective structures: an observational case study. Mon Weath Rev 32:2895–2909

Kusahara K, Hasumi H (2014) Pathways of basal meltwater from Antarctic ice shelves: a model study. J Geophys Res 119:5690–5704. doi:10.1002/2014JC009915

Labitzke K, Van Loon H (1992) On the association between the QBO and the extratropical stratosphere. J Atmos Terr Phys 54:1453–1463

Landschützer P, Gruber N, Haumann FA, Rödenbeck C, Bakker DCE, Van Heuven S, Hoppema M, Metzl N, Sweeney C, Takahashi T, Tilbrook B, Wanninkhof R (2015) The reinvigoration of the Southern Ocean carbon sink. Science 349:1221–1224. doi:10.1126/science.aab2620

Le Quéré C, Rödenbeck C, Buitenhuis ET, Conway TJ, Langenfelds R, Gomez A, Labuschagne C, Ramonet M, Nakazawa T, Metzl N, Gillett N, Heimann M (2007) Saturation of the Southern Ocean CO2 sink due to recent climate change. Science 316:1735–1738. doi:10.1126/science.1136188

Leach H, Strass V, Cisewski B (2011) Modification by lateral mixing of the warm deep water entering the Weddell Sea in the Maud rise region. Ocean Dyn 61:51–68. doi:10.1007/s10236-010-0342-y

Lechtenfeld OJ, Kattner G, Flerus R, McCallister SL, Schmitt-Kopplin P, Koch BP (2014) Molecular transformation and degradation of refractory dissolved organic matter in the Atlantic and Southern Ocean. Geochim Cosmochim Acta 126:321–337. doi:10.1016/j.gca.2013.11.009

Lenaerts JTM, van den Broeke MR, van de Berg WJ, van Meijgaard E, Kuipers Munneke P (2012) A new, high-resolution surface mass balance map of Antarctica (1979–2010) based on regional atmospheric climate modeling. Geophys Res Lett 39(L04501). doi:10.1029/2011GL050713

Lindsay R, Wensnahan M, Schweiger A, Zhang J (2014) Evaluation of seven different atmospheric reanalysis products in the Arctic. J Clim 27:2588–2606. doi:10.1175/JCLI-D-13-00014.1

Lo Monaco C, Metzl N, Poisson A, Brunet C, Schauer B (2005) Anhropogenic CO2 in the Southern Ocean: distribution and inventory at the Indian-Atlantic boundary (World Ocean Circulation Experiment line I6). J Geophys Res 110(C06010). doi:10.1029/2004JC002643

Loewe F (1972) The land of storms. Weather 27:110–121

Lumpkin R, Speer K (2007) Global Ocean overturning circulation. J Phys Oceanogr 37:2550–2562. doi:10.1175/JPO3130.1

Lüpkes C, Gryanik VM (2015) A stability-dependent parametrization of transfer coefficients for momentum and heat over polar sea ice to be used in climate models. J Geophys Res 120(2):552–581. doi:10.1002/2014JD022418

Lüpkes C, Vihma T, Birnbaum G, Wacker U (2008a) Influence of leads in sea ice on the temperature of the atmospheric boundary layer during polar night. Geophys Res Lett 35(L03805). doi:10.1029/2007GL032461

Lüpkes C, Gryanik VM, Witha B, Gryschka M, Raasch S, Gollnik T (2008b) Modeling convection over arctic leads with LES and a non-eddy-resolving microscale model. J Geophys Res 113(C09028). doi:10.1029/2007JC004099

Mantisi F, Beauverger C, Poisson A, Metzl N (1991) Chlorofluoromethanes in the western Indian sector of the Southern Ocean and their relations with geochemical tracers. Mar Chem 35:151–167

Maronga B, Gryschka M, Heinze R, Hoffmann F, Kanani-Sühring F, Keck M, Ketelsen K, Letzel MO, Sühring S, Raasch S (2015) The parallelized large-Eddy simulation model (PALM) version 4.0 for atmospheric and oceanic flows: model formulation, recent developments, and future perspectives. Geosci Model Dev 8:2515–2551. doi:10.5194/gmd-8-2515-2015

Martin JH (1990) Glacial-interglacial CO2 changes: the iron hypothesis. Paleoceanography 5:1–13

McNeil BI, Matear RJ (2008) Southern Ocean acidification: a tipping point at 450-ppm atmospheric CO2. Proc Natl Acad Sci 105:18860–18864

Meijers AJS, Klocker A, Bindoff NL, Williams GD, Marsland SJ (2010) The circulation and water masses of the Antarctic shelf and continental slope between 30 and 80°E. Deep-Sea Res II 57:723–737. doi:10.1016/j.dsr2.2009.04.019

Mensch M, Smethie WM, Schlosser P, Weppernig R, Bayer R (1998) Transient tracer observations from the western Weddell Sea during the drift and recovery of Ice Station Weddell. In: Jacobs SS, Weiss RF (eds) Ocean, ice and atmosphere: interactions at Antarctic continental margins, Ant Res Seri 75:241–256 AGU Washington

Middag R, De Baar HJW, Laan P, Cai PH, van Ooijen JC (2011a) Dissolved manganese in the Atlantic sector of the Southern Ocean. Deep-Sea Res II 58:2661–2677

Middag R, van Slooten C, De Baar HJW, Laan P (2011b) Dissolved aluminium in the Southern Ocean. Deep-Sea Res II 58:2647–2660

Millero FJ, Woosley R, Ditrolio B, Waters J (2009) Effect of ocean acidification on the speciation of metals in seawater. Oceanography 22: 72–85

Mironov DV (2009) Turbulence in the lower troposphere: second-order closure and mass-flux modelling frameworks. Lecture note in. Physics 756:161–221

Muench RD, Gunn JT, Husby DM (1990) The Weddell-scotia confluence in mid-winter. J Geophys Res 95:18177–18190

Nakayama Y, Schröder M, Hellmer HH (2013) From circumpolar deep water to the glacial meltwater plume on the eastern Amundsen shelf. Deep-Sea Res I 77:50–62

Nakayama Y, Timmermann R, Rodehacke C, Schröder M, Hellmer HH (2014) Modeling the spreading of glacial meltwater from the Amundsen and Bellingshausen seas. Geophys Res Lett 41:7942–7949. doi:10.1002/2014GL061600

Nakicenovi N, Alcamo J, Davis G, De Vries B, Fenhann J, Gaffin S, Gregory K, Grübler A, Yong Jung T, Kram T, La Rovere EL, Michaelis L, Mori S, Morita T, Pepper W, Pitcher H, Price L, Riahi K, Roehrl A, Rogner H-H, Sankovski A, Schlesinger M, Shukla P, Smith S, Swart R, van Rooijen S, Victor N, Dadi Z (2000) Special report on emissions scenarios: a special report of working group III of the intergovernmental panel on climate change. Cambridge University Press, Cambridge, U.K. 599pp

Naveira Garabato AC, McDonagh EL, Stevens DP, Heywood KJ, Sanders RJ (2002) On the export of Antarctic bottom water from the Weddell Sea. Deep-Sea Res II 49:4715–4742

Nihashi S, Ohshima KI (2015) Circumpolar mapping of Antarctic coastal polynyas and landfast sea ice: relationship and variability. J Clim 28: 3650–3670. doi:10.1175/JCLI-D-14-00369.1

Obernosterer I, Catala P, Lami R, Caparros J, Ras J, et al. (2008) Biochemical characteristics and bacterial community structure of the sea surface microlayer in the South Pacific Ocean. Biogeosciences 5:693–705

Orsi AH, Johnson GC, Bullister JL (1999) Circulation, mixing and production of Antarctic bottom water. Progr Oceanogr 43:55–109

Orsi AH, Smethie WM, Bullister JL (2002) On the total input of Antarctic waters to the deep ocean: a preliminary estimate from chlorofluorocarbon measurements. J Geophys Res 107(C8):31–31. doi:10.1029/2001JC000976

Oshima KI, Fukachami Y, Williams GD, Nihashi S, Roquet F, Kitade Y, Tamura T, Hirano D, Herraiz-Borreguero L, Field I, Hindell M, Aoki S, Wakatusucchi M (2013) Antarctic bottom water production by intense sea-ice formation in the cape Darnley polynya. Nature Geosci 6:235–240. doi:10.1038/ngeo1738

Palerme C, Kay JE, Genthon C, L'ecuyer T, Wood NB, Claud C (2014) How much snow falls on the Antarctic ice sheet? Cryosphere 8: 1577–1587. doi:10.5194/tc-8-1577-2014

Parish TR, Bromwich DH (2007) Re-examination of the near-surface air flow over the Antarctic continent and implications on atmospheric circulations at high southern latitudes. Mon Wea Rev 135:1961–1973

Paul S, Willmes S, Gutjahr O, Preußer A, Heinemann G (2015a) Spatial feature reconstruction of cloud-covered areas in daily MODIS composites. Remote Sens 7:5042–5056. doi:10.3390/rs70505042

Paul S, Willmes S, Heinemann G (2015b) Long-term coastal-polynya dynamics in the southern Weddell Sea from MODIS thermal-infrared imagery. Cryosphere 9:2027–2041. doi:10.5194/tc-9-2027-2015

Piepgras DJ, Wasserburg GJ (1982) Isotopic composition of neodymium in waters from the drake passage. Science 217:207–214. doi:10.1126/science.217.4556.207

Poisson A, Chen C-TA (1987) Why is there little anthropogenic CO_2 in the Antarctic bottom water? Deep-Sea Res 34:1255–1275

Purkey SG, Johnson GC (2010) Warming of global abyssal and deep Southern Ocean waters between the 1990s and 2000s: contributions to global heat and sea level rise budgets. J Clim 23:6336–6351

Purkey SG, Johnson GC (2012) Global contraction of Antarctic bottom water between the 1980s and 2000s. J Clim 25:5830–5844. doi:10.1175/JCLI-D-11-00612.1

Rhein M, Rintoul SR, Aoki S, Campos E, Chambers D, Feely RA, Gulev S, Johnson GC, Josey SA, Kostianoy A, Mauritzen C, Roemmich D, Talley LD, Wang F (2013) Observations: Ocean. In: Stocker TF, Qin D, Plattner G-K, Tignor M, Allen SK, Boschung J, Nauels A, Xia Y, Bex V, Midgley PM (eds) Climate change 2013: the physical science basis. Contribution of working group I to the fifth assessment report of the intergovernmental panel on climate change. Cambridge University Press, Cambridge

Riechelmann S, Schrempf M, Seckmeyer G (2013) Simultaneous measurement of spectral sky radiance by a non-scanning multidirectional spectroradiometer (MUDIS. Meas Sci Technol 24:125501. doi:10.1088/0957-0233/24/12/125501

Rigor IG, Wallace JM, Colony RL (2002) Response of sea ice to the Arctic oscillation. J Clim 15:26482663. doi:10.1175/1520-0442(2002)015<2648:ROSITT>2.0.CO;2

Rintoul SR (2007) Rapid freshening of Antarctic bottom water formed in the Indian and Pacific Oceans. Geophys Res Lett 34(L06606). doi:10.1029/2006GL028550

Rodehacke C, Hellmer HH, Beckmann A, Roether W (2007) Formation and spreading of Antarctic deep and bottom waters inferred from a chlorofluorocarbon (CFC) simulation. J Geophys Res 112(C09001). doi:10.1029/2006JC003884

Roden NP, Shadwick EH, Tilbrook B, Trull TW (2013) Annual cycle of carbonate chemistry and decadal change in coastal Prydz Bay, East Antarctica. Mar Chem 155:135–147

Rutgers van der Loeff MM, Cai P, Stimac I, Bracher A, Middag R, Klunder M, Van Heuven S (2011) ^{234}Th in surface waters: distribution of particle export flux across the Antarctic circumpolar current and in the Weddell Sea during the GEOTRACES expedition ZERO and DRAKE. Deep-Sea Res II 58:2749–2766

Schlosser P, Bayer R, Foldvik A, Gammelsrød T, Rohardt G, Münnich KO (1990) Oxygen 18 and helium as tracers of ice shelf water and winter/ice interaction in the Weddell Sea. J Geophys Res 95:3253–3263

Schlosser E, Duda MD, Powers JG, Manning KW (2008) Precipitation regime of Dronning Maud Land, Antarctica, derived from Antarctic Prediction System (AMPS) archive data. J Geophys Res 113(D24108). doi: 10.1029/2008JD009968

Schlünzen KH (1990) Numerical studies on the inland penetration of sea breeze fronts at a coastline with tidally flooded mudflats. Beitr Phys Atmos 63:243–256. doi:10.1029/2007GL032461

Schneider DP, Deser C, Okumura Y (2012) An assessment and interpretation of the observed warming of West Antarctica in the austral spring. Clim Dyn 38:323–347. doi:10.1007/s00382-010-0985-x

Schröder M, Fahrbach E (1999) On the structure and the transport of the eastern Weddell gyre. Deep-Sea Res II 46:501–527

Schröder M, Hellmer HH, Absy JM (2002) On the near-bottom variability in the northwestern Weddell Sea. Deep-Sea Res II 49:4767–4790. doi:10.1016/S0967-0645(02)00158-3

Seckmeyer G, Bais A, Bernhard G, Blumthaler M, Lantz K, Mckenzie RL, Kiedron P, Drüke S, Riechelmann S (2010) Instruments to measure solar ultraviolet radiation, part 4: Array Spectroradiometers. 43 pp, WMO-GAW report 191, TD 5038

Sexton PF, Norris RD, Wilson PA, Palike H, Westerhold T, Rohl U, Bolton CT, Gibbs S (2011) Eocene global warming events driven by ventilation of oceanic dissolved organic carbon. Nature 471:349–352. doi:10.1038/nature09826

Sloyan BM, Rintoul SR (2001) The Southern Ocean limb of the global overturning circulation. J Phys Oceanogr 31:143–173

Smetacek V, Klaas C, Strass V, Assmy P, Montresor M, Cisewski B, Savoye N, Webb A, D'ovidio F, Arrieta JM, Bathmann U, Bellerby R, Berg GM, Croot PL, Gonzalez S, Henjes J, Herndl GJ, Hoffmann LJ, Leach H, Losch M, Mills MM, Neill C, Peeken

I, Roettgers R, Sachs O, Sauter E, Schmidt M, Schwarz JN, Terbrüggen A, Wolf-Gladrow D (2012) Deep carbon export from a Southern Ocean iron-fertilized diatom bloom. Nature 487(7407): 313–319. doi:10.1038/Nature11229

Steig EJ, Schneider DP, Rutherford SD, Mann ME, Comiso JC, Shindell DT (2009) Warming of the Antarctic ice-sheet surface since the 1957 international geophysical year. Nature 457:459–462. doi:10.1038/nature07669

Steppeler J, Doms G, Schättler U (2003) Meso-gamma forecasts using the nonhydrostatic model LM. Meteorol Atmosph Phys 82:75–96

Stichel T, Frank M, Rickli J, Haley BA (2012a) The hafnium and neodymium isotope composition of seawater in the Atlantic sector of the Southern Ocean. Earth Planet Sci Lett 317-318:282–294. doi:10.1016/j.epsl.2011.11.025

Stichel T, Frank M, Rickli J, Hathorne EC, Haley BA, Jeandel C, Pradoux C (2012b) Sources and input mechanisms of hafnium and neodymium in surface waters of the Atlantic sector of the Southern Ocean. Geochim Cosmochim Act 94:22–37. doi:10.1016/j.gca.2012.07.005

Stöven T, Tanhua T, Hoppema M, Bullister JL (2015) Perspectives of transient tracer applications and limiting cases. Ocean Sci 11:699–718. doi:10.5194/os-11-699-2015

Takahashi T, Sutherland SC, Wanninkhof R, Sweeney C, Feely RA, Chipman DW, Hales B, Friederich G, Chavez F, Sabine C, Watson A, Bakker DCE, Schuster U, Metzl N, Yoshikawa-Inoue H, Ishii M, Midorikawa T, Nojiri Y, Kortzinger A, Steinhoff T, Hoppema M, Olafsson J, Arnarson TS, Tilbrook B, Johannessen T, Olsen A, Bellerby R, Wong CS, Delille B, Bates NR, De Baar HJW (2009) Climatological mean and decadal change in surface ocean pCO_2, and net sea-air CO_2 flux over the global oceans. Deep-Sea Res II 56:554–577

Tamura T, Ohshima KI, Nihashi S (2008) Mapping of sea ice production for Antarctic coastal polynyas. Geophys Res Lett 35(L07606). doi:10.1029/2007GL032903

Thoma M, Determann J, Grosfeld K, Göller S, Hellmer HH (2015) Additional sea-level rise due to projected ocean warming beneath the Filchner Rønne ice shelf: a coupled model study. Earth Planet Sci Lett 431(217–224). doi:10.1016/j.epsl.2015.09.013

Thompson DWJ, Solomon S (2002) Interpretation of recent southern hemisphere climate change. Science 296:895–899. doi:10.1126/science.1069270

Thompson DWJ, Wallace JM (2000) Annular modes in the extratropical circulation. Part I: month-to-month variability. J Clim 13:1000–1016. doi:10.1175/1520-0442(2000)013<1000:AMITEC> 2.0.CO;2

Thompson DWJ, Solomon S, Kushner PJ, England MH, Grise KM, Karoly DJ (2011) Signatures of the Antarctic ozone hole in southern hemisphere surface climate change. Nature Geosci 4:741–749. doi:10.1038/ngeo1296

Timmermann R, Hellmer HH (2013) Southern Ocean warming and increased ice shelf basal melting in the twenty-first and twenty-second centuries based on coupled ice-ocean finite-element modelling. Ocean Dyn 63:1011–1026. doi:10.1007/s10236-013-0642-0

Timmermann R, Wang Q, Hellmer HH (2012) Ice shelf basal melting in a global finite-element sea ice/ice shelf/ocean model. Ann Glaciol 53: 303–314. doi:10.3189/2012AoG60A156

Tohsing K, Schrempf M, Riechelmann S, Schilke H, Seckmeyer G (2013) Measuring high resolution sky luminance distributions with a CCD camera. Appl Opt 52:1564–1573

Tortell PD, Payne CD, Li Y, Trimborn S, Rost B, Smith WO, Risselman C, Dunbar R, Sedwick P, Di Tullio GR (2008) The CO2 sensitivity of Southern Ocean phytoplankton. Geophys Res Lett 35(L04605). doi:10.1029/2007GL032583

Trimborn S, Brenneis T, Sweet E, Rost B (2013) Sensitivity of Antarctic phytoplankton species to ocean acidification: growth, carbon acquisition and species interaction. Limnol Oceanogr 58:997–1007

Turner J, Comiso JC, Marshall GJ, Lachlan-Cope TA, Bracegirdle T, Maksym T, Meredith MP, Wang Z, Orr A (2009) Non-annular atmospheric circulation change induced by stratospheric ozone depletion and its role in the recent increase of Antarctic sea ice extent. Geophys Res Lett 36(L08502). doi:10.1029/2009GL037524

Usbeck R, Rutgers van der Loeff M, Hoppema M, Schlitzer R (2002) Shallow remineralization in the Weddell gyre. Geochemistry Geophys Geosystems 3:1–18. doi:10.1029/2001GC000182

Valkonen T, Vihma T, Kirkwood S, Johansson MM (2010) Fine-scale model simulation of gravity waves generated by Basen nunatak in Antarctica. Tellus 62A:319–332

Van Caspel M, Schröder M, Huhn O, Hellmer HH (2015) Precursors of Antarctic bottom water formed on the continental shelf off Larsen ice shelf. Deep-Sea Res I 99:1–9. doi:10.1016/j.dsr.2015.01.004

Van de Berg WJ, van den Broeke MR, van Meijgaard E, Reijmer CH (2006) Reassessment of the Antarctic surface mass balance using calibrated output of a regional atmospheric climate model. J Geophys Res 111(D11104). doi:10.1029/2005JD006495

Van de Flierdt T, Frank M, Lee D-C, Halliday AN (2002) Glacial weathering and the hafnium isotope composition of seawater. Earth Planet Sci Lett 201:639–647. doi:10.1016/S0012-821X(02)00731-8

Van den Broeke MR, Reijmer CH, van de Wal R (2004) A study of the surface mass balance in Dronning Maud Land, Antarctica, using automatic weather station. J Glaciol 50:565–582

Van Heuven SMAC, Hoppema M, Huhn O, Slagter HA, De Baar HJW (2011) Direct observation of increasing CO_2 in the Weddell gyre along the prime meridian during 1973-2008. Deep-Sea Res II 58: 2613–2635. doi:10.1016/j.dsr2.2011.08.007

Van Heuven SMAC, Hoppema M, Jones EM, De Baar HJW (2014) Rapid invasion of anthropogenic CO_2 into the deep circulation of the Weddell gyre. Phil Trans Royal Soc Lond A 372(20130056). doi:10.1098/rsta.2013.0056

Van Lipzig NPM, King JC, Lachlan-Cope TA, van den Broeke MR (2004) Precipitation, sublimation, and snow drift in the Antarctic Peninsula region from a regional atmospheric model. J Geophys Res 109(D24106). doi:10.1029/2004JD004701

Venchiarutti C, Rutgers van der Loeff M, Stimac I (2011) Scavenging of 231 Pa and thorium isotopes based on dissolved and size-fractionated particulate distributions at drake passage (ANTXXIV-3). Deep-Sea Res II 58:2767–2784. doi:10.1016/j.dsr2.2010.10.040

Vihma T, Pirazzini R, Fer I, Renfrew IA, Sedlar J, Tjernström M, Lüpkes C, Nygard T, Notz D, Weiss J, Marsan D, Cheng B, Birnbaum G, Gerland S, Chechin D, Gascard JC (2014) Advances in understanding and parameterization of small-scale physical processes in the marine Arctic climate system: a review. Atmos Chem Phys 14: 9403–9450. doi:10.5194/acp-14-9403-2014

Wacker U, Potty K, Lüpkes C, Hartmann J, Raschendorfer M (2005) A case study on a polar cold air outbreak over Fram Strait using a mesoscale weather prediction model. Bound-Layer Meteorol 117: 301–336. doi:10.1007/s10546-005-2189-1

Wacker U, Ries H, Schättler U (2009) Precipitation simulation for Dronning Maud land using the COSMO model. Ant Sci 21:643–662

Waugh DW, Primeau F, Devries T, Holzer M (2013) Recent changes in the ventilation of the Southern Ocean. Science 339:568–570. doi:10.1126/science.1225411

Welker C, Martius O, Froidevaux P, Reijmer CH, Fischer H (2014) A climatology analysis of high-precipitation events in Dronning Maud land, Antarctica, and associated large-scale atmospheric conditions. J Geophys Res 119:11,932–11,954. doi:10.1002/2014JD022259

Weppernig R, Schlosser P, Khatiwala S, Fairbanks RG (1996) Isotope data from Ice Station Weddell: implications for deep water formation in the Weddell Sea. J Geophys Res 101:25723–25739

Whitworth T III, Nowlin WD Jr, Orsi AH, Locarnini RA, Smith SG (1994) Weddell Sea shelf water in the Bransfield Strait and

Weddell-scotia confluence. Deep-Sea Res I 41:629–641. doi:10.1016/0967-0637(94)90046-9

Wittmann AC, Portner H-O (2013) Sensitivities of extant animal taxa to ocean acidification. Nature. Clim Chang 3:995–1001. doi:10.1038/nclimate1982

WMO (World Meteorological Organization) (2014) Scientific assessment of ozone depletion: 2014, Global Ozone Research and Monitoring Project – Report No. 55 416 pp Geneva Switzerland

Wuttke S, Seckmeyer G (2006) Spectral radiance and sky luminance in Antarctica: a case study. Theor Appl Climatol 85:131–148. doi:10.1007/s00704-005-0188-2

Wuttke S, Seckmeyer G, Koenig-Langlo G (2006) Measurements of spectral snow albedo at Neumayer, Antarctica. Ann Geophys 24: 7–21

Wyngaard JC (2004) Toward numerical modeling in the "Terra incognita. J Atmos Sci 61:1816–1826. doi:10.1175/1520-0469

Xin Y, Rinke A, Bian L, Dethloff K, Xiao C, Mielke M (2010) Climate and forecast mode simulations for Antarctica: implications for temperature and wind. Adv Atm Sci 27:1453–1472. doi:10.1007/s00376-010-9178-0

Xue Z, Rehkämper M, Horner TJ, Abouchami W, Middag R, van de Flierdt T, De Baar HJW (2013) Cadmium isotope fractionation in the Southern Ocean. Earth Planet Sci Lett 382:161–172

Zaengl G (2005) The impact of lee-side stratification on the spatial distribution of orographic precipitation. Q J R Meteorol Soc 131:1075–1091

Zhao Y, Vance D, Abouchami W, De Baar HJW (2014) Biogeochemical cycling of Zn and its isotopes in the Southern Ocean. Geochim Cosmochim Acta 125:653–672